The Iowa State College Bulletin

MOMENT CONTOURS FOR BRIDGE ABUTMENT WINGWALLS OF CONSTANT THICKNESS

by C. L. Hulsbos
W. H. McCasland

IOWA ENGINEERING EXPERIMENT STATION

Iowa State College
Ames, Iowa

THE IOWA ENGINEERING EXPERIMENT STATION

The Iowa Engineering Experiment Station was organized in 1904 for the purpose of conducting investigations that would aid in the industrial development of the area, and for carrying on an experimental program on engineering problems encountered in public administration.

The Station is engaged in the investigation of fundamental engineering problems, and in the development of industrial processes to utilize further the raw materials of the area or to develop products of use to the people of the state and nation. This work is carried on in the fields of agriculture, chemical, civil, ceramic, electrical, mechanical and aeronautical engineering and theoretical and applied mechanics.

The cooperation and facilities of the Station are offered to industries within and without the State in furtherance of the objectives stated above. For further information address

THE IOWA ENGINEERING EXPERIMENT STATION
IOWA STATE COLLEGE
AMES, IOWA

GEORGE R. TOWN, *Director*
DAVID R. BOYLAN, *Associate Director*
JOHN H. BOLTON, *Editor*

MOMENT CONTOURS FOR BRIDGE ABUTMENT WINGWALLS OF CONSTANT THICKNESS

by

C. L. Hulsbos, Professor of Civil Engineering

and

W. H. McCasland, Formerly Graduate Assistant,

Iowa Engineering Experiment Station

Price: Seventy-five cents

TABLE OF CONTENTS

Moment Contours For Bridge Abutment Wingwalls of Constant Thickness

FOREWORD

Iowa Engineering Experiment Station Bulletins 182, 183 and 184 are the final report on a project on bridge abutment wingwalls of the flared type. The project has been sponsored by the Iowa Highway Research Board of the Iowa State Highway Commission.

Bulletin 182 reported the first two phases of the project. Phase one included a comprehensive literature review and a questionnaire survey. Phase two included the results of a study to establish a feasible analytical method for the solution of this type of plate problem.

This bulletin (#183) presents design data for wingwalls of constant thickness. These design data are in the form of moment contours for wingwalls of the various proportions being used by the Iowa State Highway Commission.

Bulletin 184 will provide an analytical procedure for the structural analysis of wingwalls of variable thickness. As an example a typical variable thickness wingwall will be analyzed for moments which will be presented as moment contours.

NOTATION AND DEFINITIONS

NOTATION

a	Base length of wingwall in feet
b	Height of outside vertical wingwall edge in feet
C	Numerical value of moment contour
d	Vertical distance from footing boundary in inches
e	Normal unit strain
e_u	Maximum principal unit strain
e_v	Minimum principal unit strain
E	Modulus of elasticity in tension and compression
E_a	Modulus of elasticity for aluminum
E_c	Modulus of elasticity for concrete
ft	Feet
G	Modulus of elasticity in shear, modulus of rigidity
G_a	Modulus of rigidity for aluminum
G_c	Modulus of rigidity for concrete
h	Thickness of wingwall or plate
I	Moment of inertia of a plate section of unit edge length
in	Inches
J	Torsional constant for a rectangular section corresponding to polar moment of inertia for circular sections
k	A dimensionless constant
lb	Pound
M	Bending moment
M_u	Maximum principal bending moment
M_v	Minimum principal bending moment
M_x, M_y	Bending moment with respect to x and y axes
M_{xy}	Torsional moment with respect to rectangular coordinates
p	Intensity of a distributed load
p_f	Intensity of a disturbed load at fixed-fixed corner
psi	Pounds per square inch
psf	Pounds per square foot

w	Deflection of plate normal to middle plane
x, y, z	Rectangular coordinates
λ	Finite difference grid spacing in inches
μ	Poisson's ratio
μ_a	Poisson's ratio for aluminum
μ_c	Poisson's ratio for concrete
σ	Unit stress
σ_u	Maximum principal unit stress
σ_v	Minimum principal unit stress
Θ_x	Direction of maximum principal moment with respect to x-axis
φ	Rotation of outer free edge of wingwall at the footing boundary with respect to an axis along that boundary

D	Plate stiffness,	$\dfrac{Eh^3}{12(1 - \mu^2)}$
H		$-D/\lambda^2$
K		$\dfrac{p_f\, a^2}{10^4}$
N		$\dfrac{D(1 - \mu)}{4\lambda^2}$

DEFINITIONS

Back face of wingwall—Side adjacent to fill

Front face of wingwall—Side opposite back face

Fixed-fixed corner—Corner of wingwall at juncture of breastwall and footing boundaries

Positive moment—Bending moment producing tension on front face

Positive direction of maximum principal moment — Direction of stress caused by maximum principal moment measured clockwise to x-axis when viewed from within backfill

INTRODUCTION

OBJECTIVES

A bridge abutment wingwall is an integral and often necessary part of a bridge structure. Its purpose is to serve as a retaining wall for the approach fill and as a counterfort for the breastwall. It also acts as a water baffle to prevent scouring of the fill from behind the abutment. The wingwalls may be designed with a constant or variable thickness and may be built with or without counterforts. Wingwalls are often rigidly connected to both the footing and breastwall. This study is restricted to constant thickness wingwalls without counterforts which are assumed to be rigidly connected to the footing and breastwall (figure 1).
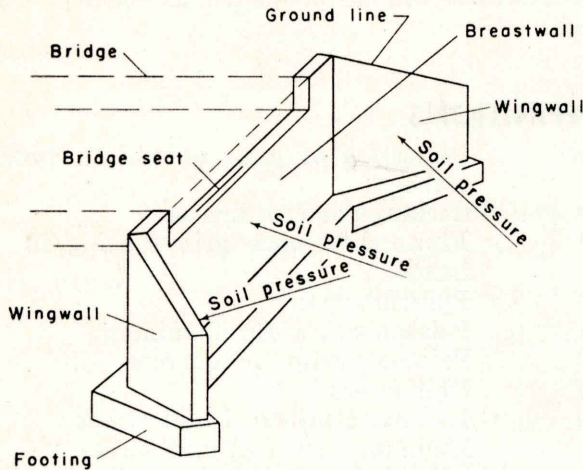

Fig. 1. Reinforced concrete bridge abutment.

In the design of a structure such as a wingwall a knowledge of the bending moments involved is of primary importance. The analysis of the moments in a wingwall is a complicated problem. The average engineer has neither the time nor the equipment available for its solution; in fact an exact mathematical analysis is almost impossible to attain. Designs in the past have been based, for the most part, on experience or empirical rules.

This project, which is being conducted by the Iowa Engineering Experiment Station, is divided into four parts. Part one of the project began in 1954 and is an extensive review of all available material published. In this review no information of significance was found. The Portland Cement Association [8, p. 12], stated with reference to wingwalls, ". . . no structural analysis is available by which the stresses may be determined". In the hope that unpublished information might be in use by some engineering organization a questionnaire was sent to all state highway commissions, to many consulting firms in the United States and Canada, and to all railroads that were American Railway Engineering Association members. Seventy percent of the questionnaires were returned, but none of the answers gave any information on a rational analysis of the problem.

Part two of the project, an experimental and theoretical investigation was then made. When an exact mathematical solution of the problem did not prove feasible, an investigation of available numerical methods was made. One of these methods, finite differences, was chosen as the most suitable means of solution. A determination of the necessary size of the infinite intervals used in the equations and a check on the method's accuracy was made with the aid of experimental tests conducted on a model aluminum wingwall.

Parts one and two are reported in Bulletin 182 of the Iowa Engineering Experiment Station. Part three of the project, which is this investigation, has several objectives:

1. Further experimental verification of the finite difference theory by tests conducted on a model aluminum wingwall of a different size proportion as that investigated in part two of the project. (See figure 2 for wingwall size ratios investigated.)

Wingwall number	Size ratio	
1	$\frac{b}{a} = \frac{2}{3}$	
2	$\frac{b}{a} = \frac{4}{5}$	
3	$\frac{b}{a} = 1$	
4	$\frac{b}{a} = \frac{5}{4}$	
5	$\frac{b}{a} = \frac{3}{2}$	

Fig. 2. Wingwall size ratios investigated.

2. Development of bending moment contours and the determination of an equation which when used with the contours will enable the calculation of moment at any point within the wingwall.

3. Investigation of wingwall footing rotation and its resulting effect on the bending moments.

4

REVIEW OF LITERATURE

Little information of value was located in the review made in 1954, and no mathematical analysis for the moments in a wingwall was found. The material included in the publications was based on past experience and empirical rules. Diagrams were given, [4] showing typical placement of reinforcing. Several coefficients for moments for a U-shaped wingwall are published [11]. However, there is no indication that these coefficients come from any rational analysis. Chettoe and Adams [2 facing p. 288] gave an illustration showing a ten-
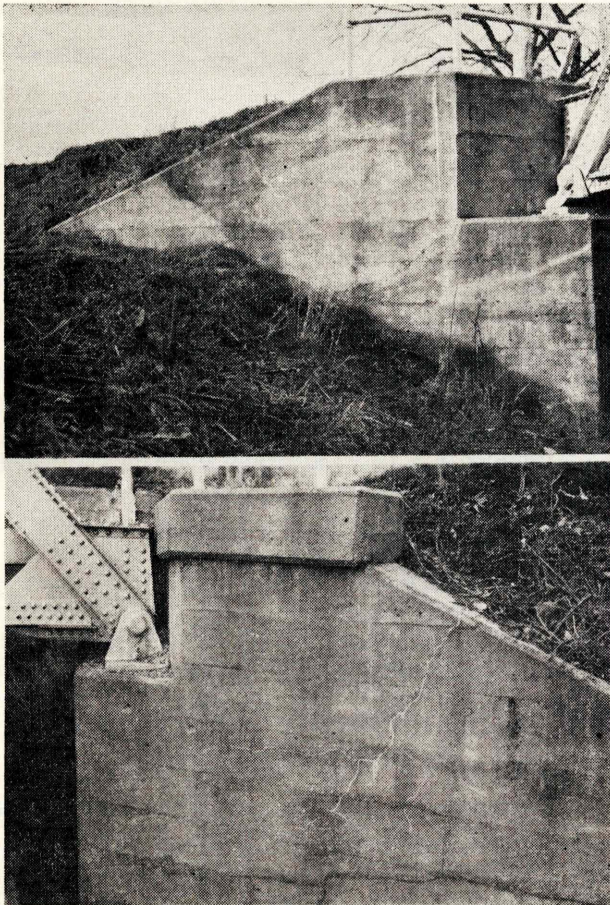

Fig. 3. Cracks in wingwalls.

sion crack on the side of the wingwall facing the bridge superstructure. They recommend the inclusion of bars running diagonally across that side but give no indication of steel quantities. Similar cracks on wingwalls (figure 3) were found on several bridges across the Skunk River near Ames, Iowa. The Portland Cement Association [8, pp. 10, 12] states, "The joint section between breastwall and wingwall is difficult to analyze, and the safe and economical amount of reinforcement can seldom be calculated, . . . suitable reinforcement may be provided—by judgment or empirical rules — in the conventional type of abutment . . ."

The possibility of an exact mathematical analysis was investigated as reported in Bulletin 182[3]. For this analysis the wingwalls were assumed to be thin homogeneous plates. A mathematical solution involved finding an expression to satisfy the Lagrange differential plate equation and all boundary conditions. Because of the unusual nature of the boundaries such an analysis was considered by mathematicians to be nearly impossible. An analysis by finite differences was found to be most expedient, but this method was not without its difficulties. In the use of finite differences a grid pattern which controls the finite interval of the equations had to be established. The practical size of this interval with its resulting number of equations was found by an experimental theoretical comparison. Sets of equations for several different grid spacings were written for one plate size, and the results of these equations were checked against experimental studies made on an aluminum wingwall model of the same plate dimensions. The results of the tests indicated that a grid pattern giving thirty to forty linear simultaneous equations was sufficiently accurate.

The method of analysis was thus formulated. Its subsequent application to the determination of bending moments in wingwalls of various size ratios is reported in this publication.

THEORETICAL INVESTIGATION

LAGRANGE PLATE EQUATION

The Lagrange plate equation [9, 12, 13] is the governing equation for small deflections of thin, constant thickness plates. The equation can be expressed as follows:

$$\frac{\partial^4 w}{\partial x^4} + 2\frac{\partial^4 w}{\partial x^2 \partial y^2} + \frac{\partial^4 w}{\partial y^4} = \frac{p}{D}; \text{ in which}$$

w = deflection normal to middle plane of plate

x, y = coordinates in plane of plate

p = distributed pressure normal to plate

D = plate stiffness $\dfrac{Eh^3}{12(1-\mu^2)}$

In the derivation of the Lagrange equation for thin plates certain assumptions are made:

1. The normals of the middle plane before bending are deformed into the normals of the middle plane after bending.
2. The stress σ_z is small compared with the other stress components and may be neglected.
3. The middle plane remains unstrained after bending.

A solution of the equation involves finding an expression for the deflection w in terms of the rectangular coordinates x and y which satisfies the Lagrange equation and all boundary conditions. Once such equation for the deflections has been found the bending moments in any direction may be determined. The moment is proportional to

the curvature or second partial derivitive of deflection with respect to the coordinates in the plane of the plate. Poisson's ratio must be taken into consideration because the plate forms a bi-dimensional stress condition. Mathematically the bending and twisting moments may be expressed as follows [12, 13]:

$$M_x = - D \left(\frac{\partial^2 w}{\partial x^2} + \mu \frac{\partial^2 w}{\partial y^2} \right)$$

$$M_y = - D \left(\frac{\partial^2 w}{\partial y^2} + \mu \frac{\partial^2 w}{\partial x^2} \right)$$

$$M_{xy} = M_{yx} = D (1 - \mu) \frac{\partial^2 w}{\partial x \partial y}$$

Closed and series solutions of the Lagrange equation have been found for several types of plates with various boundary conditions. These solutions have generally been for symmetrical plates with symmetrical boundaries. The solution of a plate problem representing a wingwall in which two adjacent edges are clamped and the other two, one of which is sloping, remain free was considered by mathematicians to be practically impossible.

FINITE DIFFERENCE METHOD

Since closed and series solutions were not feasible, the problem was to find a rational means of analysis for the wingwalls. Several numerical methods for the approximate solution of plates have been investigated [3]. The method of solution by finite differences [10, 13] was found to be the most simple and direct procedure for application to this particular problem.
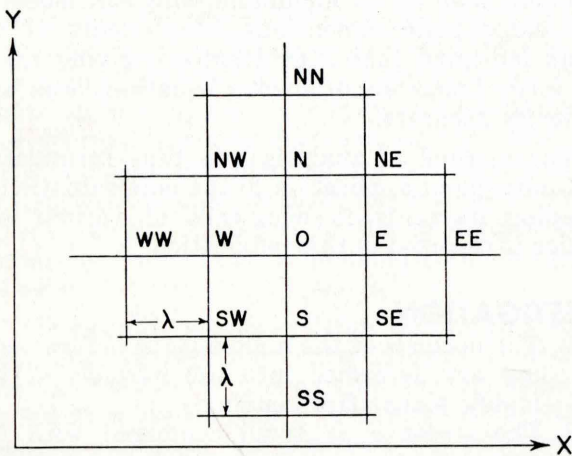
The method of finite differences consists essentially of replacing the governing differential equation and equations defining boundary conditions with their respective finite difference equations. The method requires the selection of a grid system in the plane of the plate whose spacing between grid lines controls the finite interval of the equations. One equation is written for each grid intersection. Each equation is in terms of the appropriate finite difference coefficients for

each grid point within an immediate area multiplied by the unknown deflection at the particular grid intersections. Mathematically this may be demonstrated as follows: Consider point o located within the network of grid intersections.

For point o the Lagrange differential equation is

$$\frac{\partial^4 w}{\partial x^4} + 2 \frac{\partial^4 w}{\partial x^2 \partial y^2} + \frac{\partial^4 w}{\partial y^4} = \frac{P_o}{D}$$

The finite difference expressions for the partial derivatives of the above equation are: [13]

$$\left(\frac{\partial^4 w}{\partial x^4} \right)_o = \frac{1}{\lambda^4} (w_{EE} - 4w_E + 6w_o - 4w_W + w_{WW})$$

$$\left(\frac{\partial^4 w}{\partial y^4} \right)_o = \frac{1}{\lambda^4} (w_{SS} - 4w_S + 6w_o - 4w_N + w_{NN})$$

$$\left(\frac{\partial^4 w}{\partial x^2 \partial y^2} \right)_o = \frac{1}{\lambda^4} \left[w_{NE} + w_{SE} + w_{SW} + w_{NW} \right.$$
$$\left. - 2 (w_N + w_S + w_E + w_W) + 4w_o \right]$$

Substituting into the Lagrange equation and collecting terms,

$$20w_o - 8 (w_N + w_E + w_S + w_W)$$
$$+ 2 (w_{NE} + w_{SE} + w_{SW} + w_{NW})$$
$$+ w_{NN} + w_{EE} + w_{SS} + w_{WW} = \frac{P_o \lambda^4}{D}$$

gives the finite difference equation for the deflection of point o. The term $\frac{\lambda^4}{D}$ is a constant for the plate, and the distributed pressure p_o at each node point can be found. Their substitution leaves only the various deflections as unknowns in the equation. Similar expressions are written for adjacent points with appropriate changes made to satisfy the various boundary conditions. The result is a series of linear simultaneous equations whose unknowns are the deflections of the node points. The number of equations corresponds with the number of grid intersections on the plate. A solution of the simultaneous equations gives the unknown deflections at each node point.

The sloping edge of the wingwall presented a problem in the fitting of the rectangular mesh system to that boundary. A simplifying assumption was made in which the trapezoidal plates were replaced with rectangular ones. The normal loading remained the same, increasing linearly with depth from the now imaginary sloping edge (figure 4). The replacement of the sloping edge by a boundary passing horizontally through
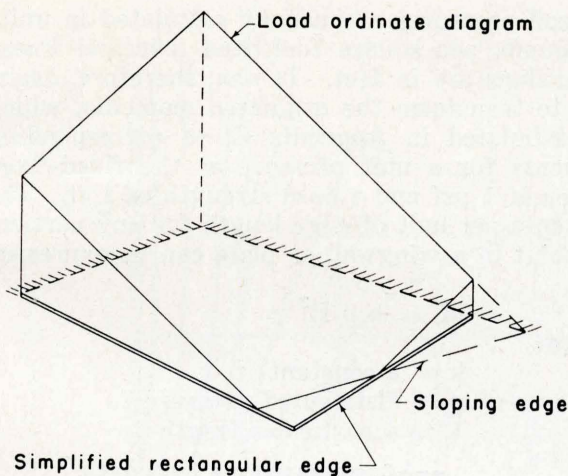
Fig. 4. Loading diagram with approximation for sloping edge.

the approximate mid-point of the original edge appeared to be a reasonable approximation. The simplification was made in a region of low pressure ordinates, and the changes in plate stiffness by this alteration were small. The validity of the assumption was proved satisfactory in the experimental tests.

The results of the tests previously made [3] indicated that a grid spacing resulting in thirty to forty linear simultaneous equations was sufficiently accurate. Using this information, one set of simultaneous equations was written for each of the four remaining plates. Each set contained thirty to forty independent equations, the exact number depending on the particular plate size. The results of the 7 x 7 grid pattern were used for wingwall No. 2 of figure 2.

BENDING MOMENT ANALYSIS

At an interior point, for example, the moments in the x and y directions and the twisting moments were evaluated by substitution of the deflections into the following finite difference equations for moment [1]:

$$M_x = - \frac{D}{\lambda^2}\left[w_W + w_E + \mu\,(w_N + w_S) - (2 + 2\mu)\,w_0\right]$$

$$M_y = - \frac{D}{\lambda^2}\left[w_N + w_S + \mu\,(w_E + w_W) - (2 + 2\mu)\,w_0\right]$$

$$M_{xy} = \frac{D\,(1 - \mu)}{4\lambda^2}\,(w_{SE} - w_{NE} - w_{SW} + w_{NW})$$

The principal moments were found by the Mohr graphical solution of the principal moment equation [1]:

$$M_{u,v} = \frac{M_x + M_y}{2} \pm \sqrt{\left(\frac{M_x - M_y}{2}\right)^2 + (M_{xy})^2}$$

Directions of the principal moments were determined by the equation [1].

$$\text{Tan } 2\,\theta = \frac{2M_{xy}}{M_x - M_y}$$

A solution of the equations for twisting moment along the free edges gives a finite value, as may be observed in Appendix C. This is in agreement with the assumptions made in the derivation of the dfferential plate equation and is the best that can be obtained unless an equation of higher order is used. Three boundary conditions are known to hold true, that is, the vertical edge force Q, twisting moment, M_{xy}, and normal M_n must be zero. However, it has been shown that only two conditions are required to satisfy the free boundary [13]. One of these is established by setting the normal moment equal to zero. The twisting moment along the boundary can be replaced by two vertical forces of magnitude, M_{xy}, at an elemental distance dy apart. This substitution produces a couple $(M_{xy})\,(dy)$. Adjacent to this element is another couple of different magnitude $(M_{xy} + \frac{\partial M_{xy}}{\partial y}dy)\,dy$. A summation of forces at their common point gives $\frac{\partial M_{xy}}{\partial y}\,dy$ or a distributed force per unit length of $\frac{\partial M_{xy}}{\partial y}$. A final boundary condition stating that all edge forces must be zero can then be written as

$$V = Q - \frac{\partial M_{xy}}{\partial y} = 0$$

where:

$Q =$ vertical edge force per unit of length

$\frac{\partial M_{xy}}{\partial y} =$ distributed vertical edge force per unit of length resulting from twisting moment transformation.

As can be noted the sum of the edge force Q and the partial of the twisting moment with respect to the tangential direction, $\frac{\partial M_{xy}}{\partial y}$ has replaced the exact conditions, $Q = 0$ and $M_{xy} = 0$. Therefore a finite value of M_{xy} on the free border resulting from the solution of the equations can be understood. The replacement of the twisting moment by vertical edge forces affects the stress distribution only in the immediate region of the edge. This necessary substitution can be attributed to the assumption that the normals to the middle plane before bending remain normal after bending. Without this assumption a sixth order equation can be developed for which three equations are then necessary for satisfying a free boundary. For thin plates with small deflections the sixth order differentials are of little consequence and may be neglected. We have remaining the fourth order Lagrange partial differential equation. As

a conservative procedure a principal moment was evaluated at each grid point along the free edge using the tangential moment and twisting moment.* Its direction was assumed tangential to the edge, as is known to be true.

MOMENT CONTOURS AND TRAJECTORIES

All moments were evaluated for the five wing-wall size ratios for a base or a length of 3 feet and pressure ordinate at the fixed-fixed corner of 1 psi. These dimensions correspond with the dimension of the experimental test plate. In the practical design of a bridge abutment wingwall, however,

---

*The normal moment was zero as defined in the boundary condition.

the soil pressures are usually calculated in units of pounds per square foot, and principal linear dimensions are in feet. It was, therefore, desirable to transform the evaluated moments, which are tabulated in Appendix C, to corresponding moments for a unit pressure at the fixed-fixed corner of 1 psf and a base strength of 1 ft. The moments per unit of edge length for any particular point in a wingwall or plate can be expressed by

$$M = k\,p\,L^2$$

where:

k = a constant
p = distributed pressure
L = a particular length

- - - Compression on back face
——— Tension on back face

Fig. 5. Maximum principal moment contours giving values of coefficient "C".

Fig. 6. Maximum principal moment trajectories.

- - - Compression on back face
——— Tension on back face
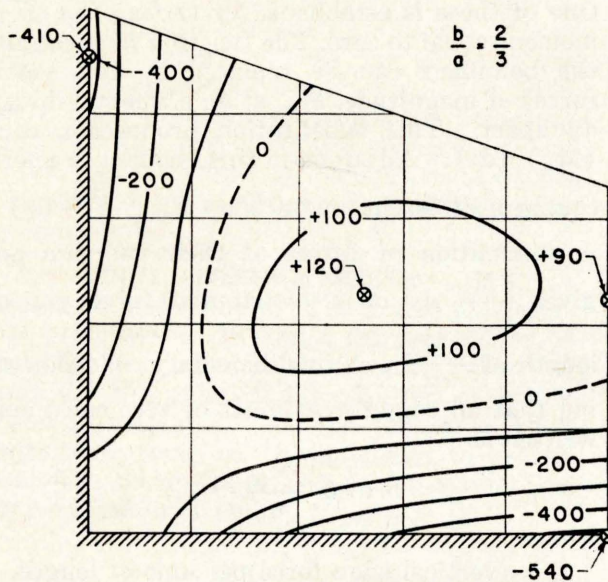

Fig. 7. Maximum principal moment contours giving value of coefficient "C".
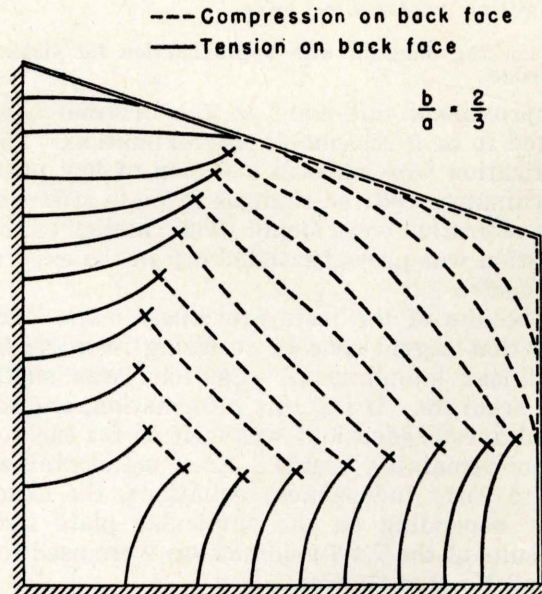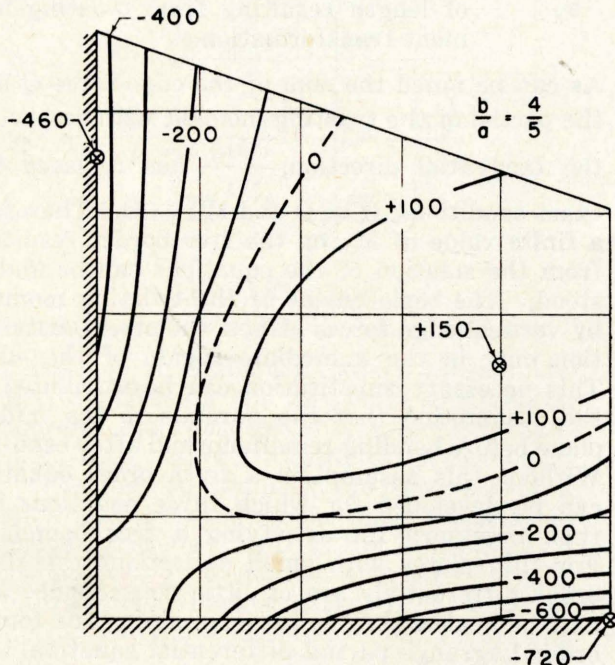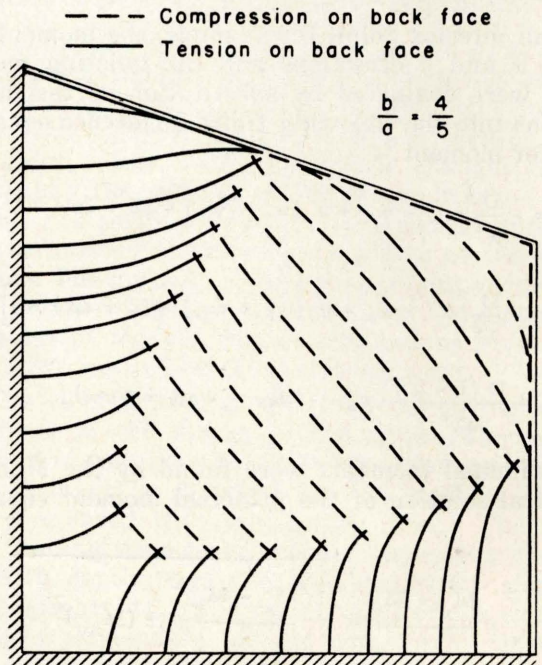

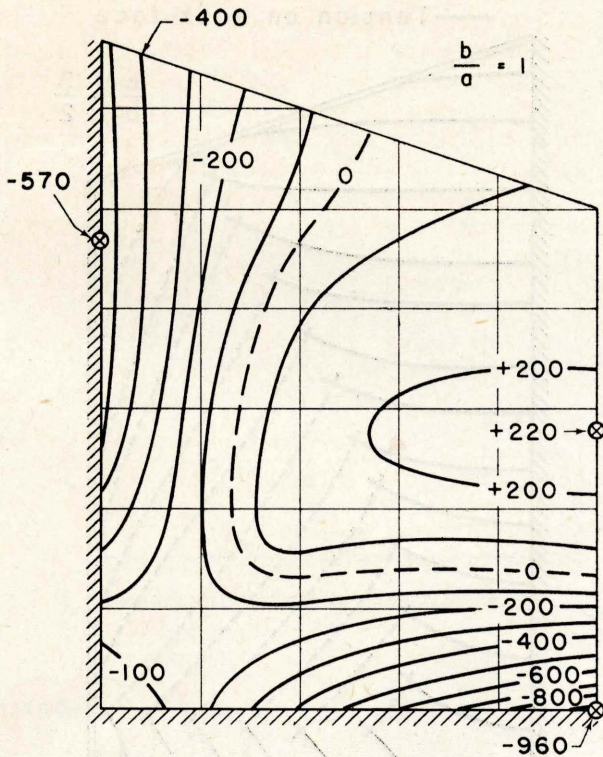Fig. 8. Maximum principal moment trajectories.

8

Fig. 9. Maximum principal moment contours giving values of coefficient "C".
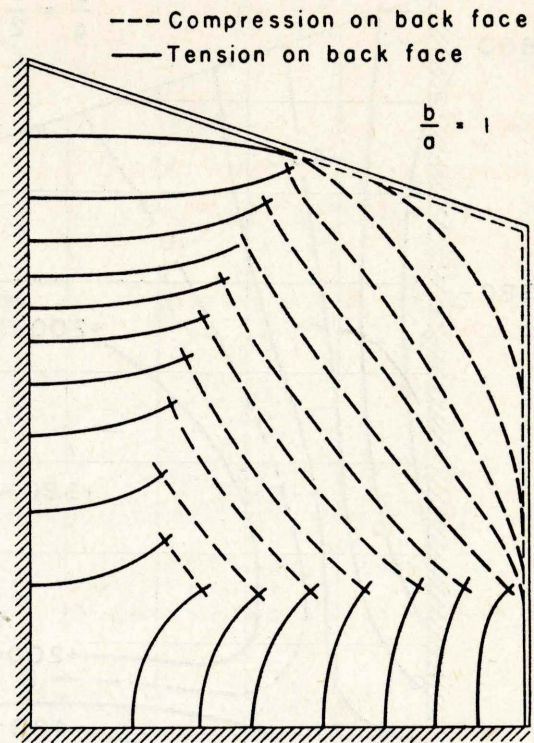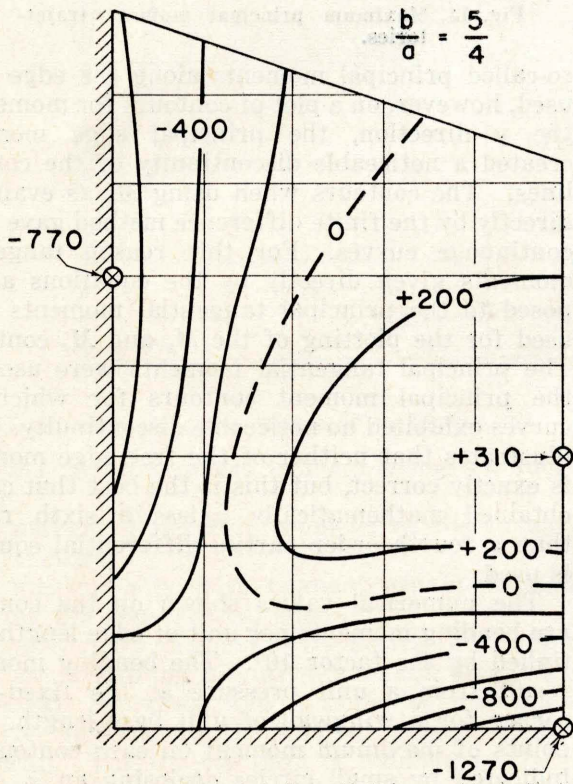

Fig. 10. Maximum principal moment trajectories.

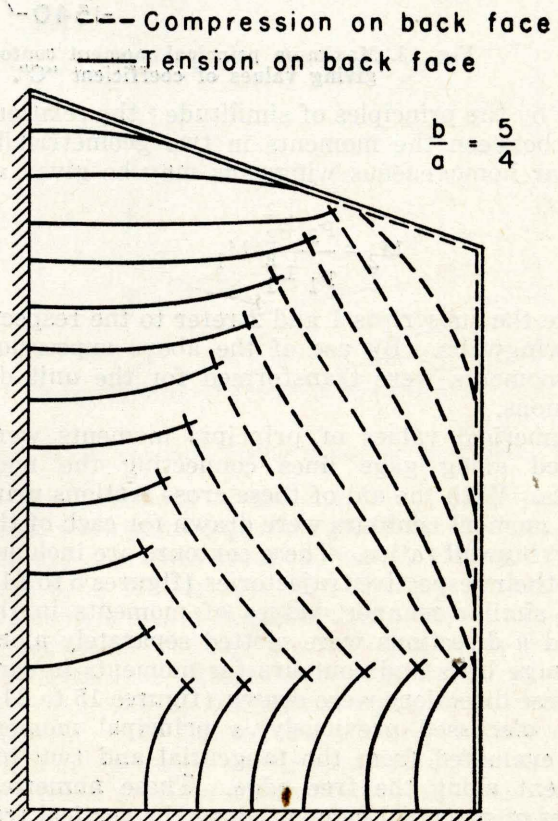Fig. 11. Maximum principal moment contours giving values of coefficient "C".

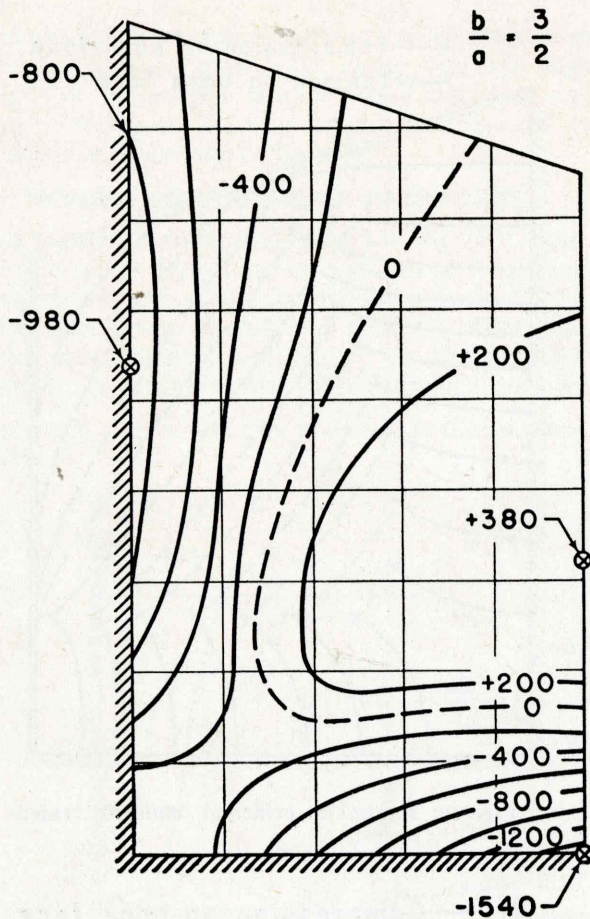Fig. 12. Maximum principal moment trajectories.

9

$$\frac{b}{a} = \frac{3}{2}$$

Fig. 13. Maximum principal moment contours giving values of coefficient "C".

$$\frac{b}{a} = \frac{3}{2}$$

Fig. 14. Maximum principal moment trajectories.

Then by the principles of similitude [6] the relationship between the moments in two geometrically similar homogeneous wingwalls may be given as

$$M_2 = \frac{p_2 \, L_2^2}{p_1 \, L_1^2} \, M_1$$

where the subscripts 1 and 2 refer to the respective wingwalls. By use of the above expression the moments were transformed for the unit dimensions.

Numerical values of principal moments were plotted along gage lines connecting the node points. With the aid of these cross sections principal moment contours were drawn for each of the five wingwall ratios. These contours are included with their respective trajectories (figures 5 to 14). In a similar manner, values of moments in the x and y directions were plotted separately along the gage lines and contours for moments in each of these directions were drawn (figures 15 to 24).

As discussed previously, a principal moment was evaluated from the tangential and twisting moment along the free edge. These numerical values of principal moment along the vertical free edge, for example, and the values of moment in the y direction for that edge should be identically equal for any particular wingwall. When the
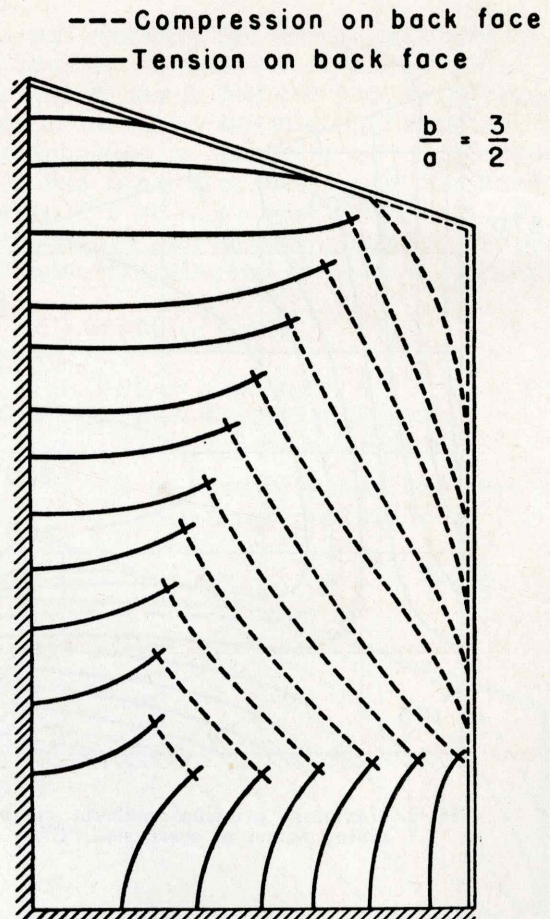
so-called principal moments along the edge were used, however, on a plot of contours for moment in the y direction, the principal edge moments created a noticeable discontinuity of the contour lines. The contours when using M_y as evaluated directly by the finite difference method gave more continuous curves. For this reason tangential moments given directly by the equations as opposed to the principal tangential moments were used for the plotting of the M_y and M_x contours. The principal tangential moments were used for the principal moment contours for which the curves exhibited no noticeable discontinuity. This illustrates that neither of the free edge moments is exactly correct, but this is the best that can be obtained mathematically unless a sixth rather than a fourth order partial differential equation is used.

The numerical values shown on the contours are bending moments per unit of edge length multiplied by the factor 10^4. The bending moments result from a unit pressure at the fixed-fixed corner for a wingwall of unit base length. The points of maximum moment on each contour are indicated by small circles enclosing an x. (See for example, figure 5). For each principal moment contour there are three points of maximum moment:

10

Fig. 15. M_x contours giving values of coefficient "C".
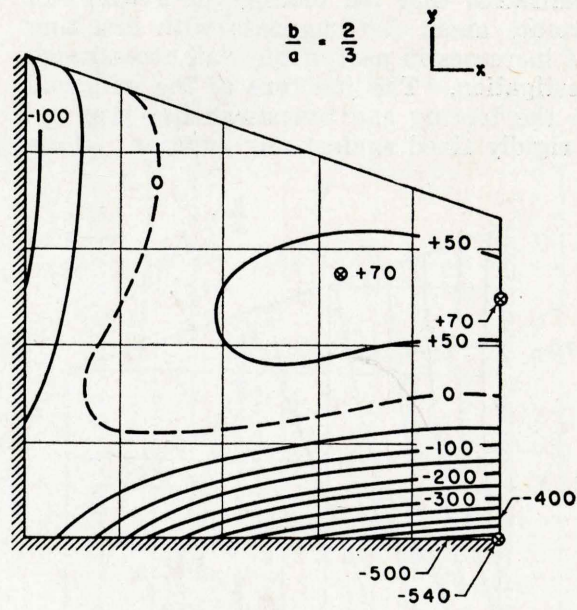
Fig. 16. M_y contours giving values of coefficient "C".

Fig. 17. M_x contours giving values of coefficient "C".
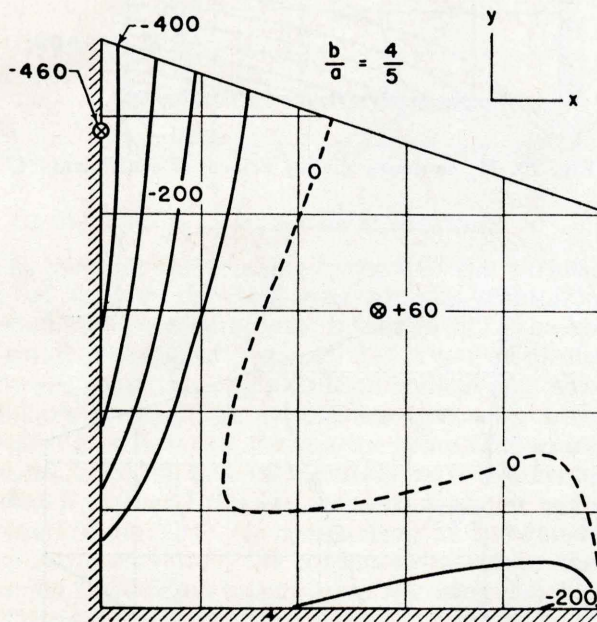
Fig. 18. M_y contours giving values of coefficient "C".

1. A maximum negative moment along the footing.
2. A maximum negative moment at the breastwall juncture.
3. A maximum positive moment usually located along the free vertical edge.

The contours for moment in the x direction have a point of maximum negative moment along the breastwall boundary and a point of maximum positive moment in the central region of the wingwall. For the contours of moment in the y direction there are points of maximum moment along the footing boundary and in the central region or on the vertical free edge.
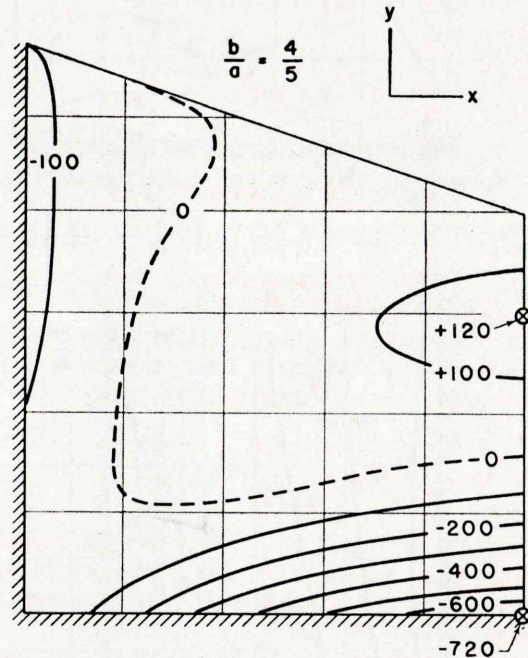
The directions of the maximum principal moment were plotted at each grid intersection allowing the construction of moment trajectories (figures 6, 8, 10, 12, 14). By *direction of principal moment* is meant the direction normal to the axis about which bending occurs. Or it can be visualized as the direction of maximum principal stress caused by the maximum principal bending moment. The dashed trajectories indicate maximum compression on the back face; the solid lines represent maximum tension on that face. At the point where maximum compression changes to maximum tension the trajectories, of course, cross at right angles.

FOOTING ROTATION

A realization that the footing for a wingwall could rotate about its long axis with resulting moment increases in part of the wall necessitated an investigation. The juncture of the wingwall to both the footing and breastwall has been assumed rigidly fixed against any rotation. How-ever, it is known there will be a certain limited amount of rotation of the footing, since no foundation can be absolutely rigid. This rotation will cause an increase of both negative moment at the breastwall and positive moment in the central region, and of course a reduction of negative moment along the footing.
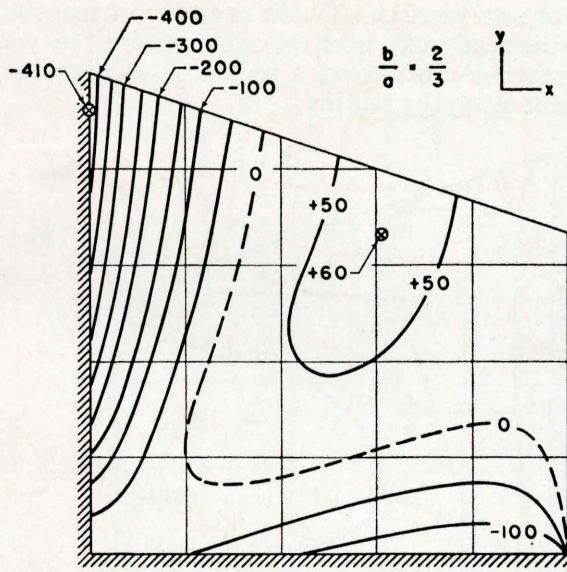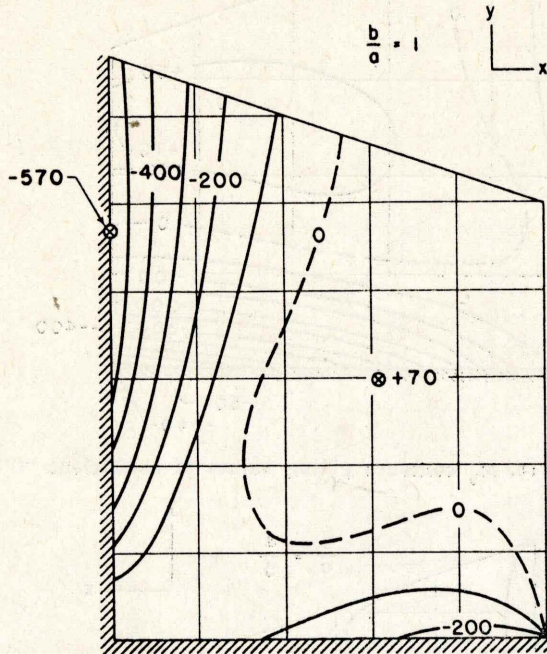
Fig. 19. M_x contours giving values of coefficient "C".
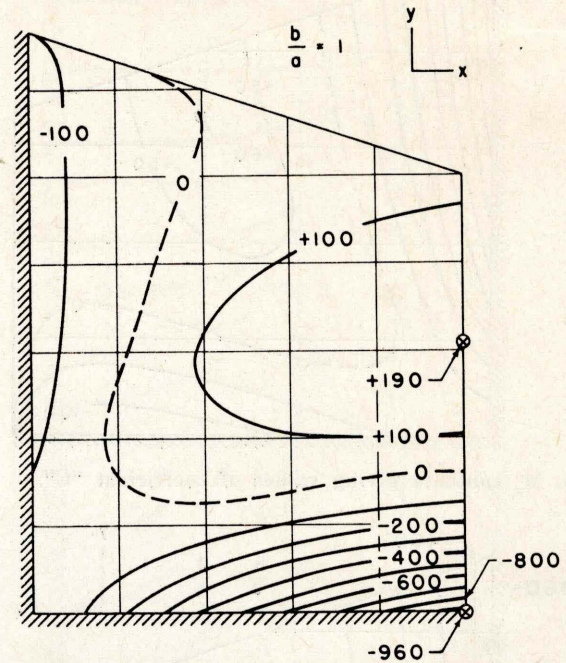
Fig. 20. M_y contours giving values of coefficient "C".
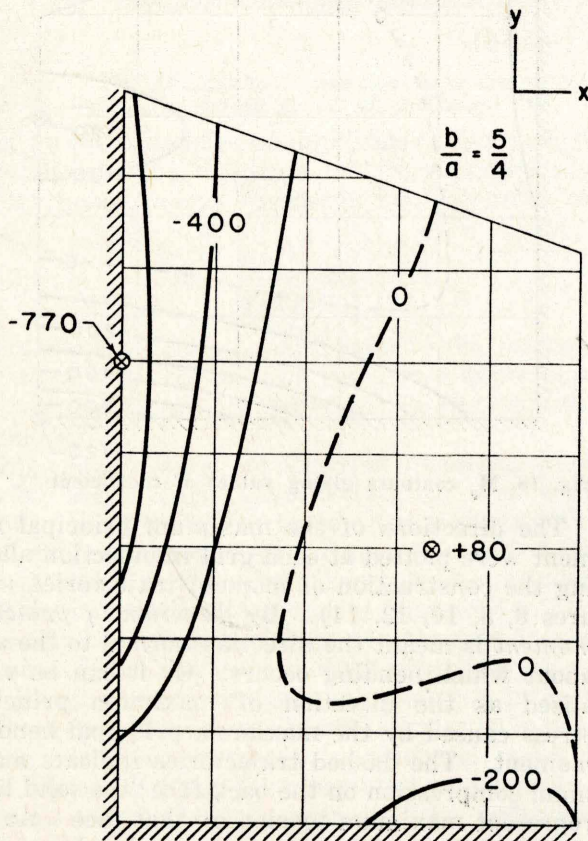
Fig. 21. M_x contours giving values of coefficient "C".
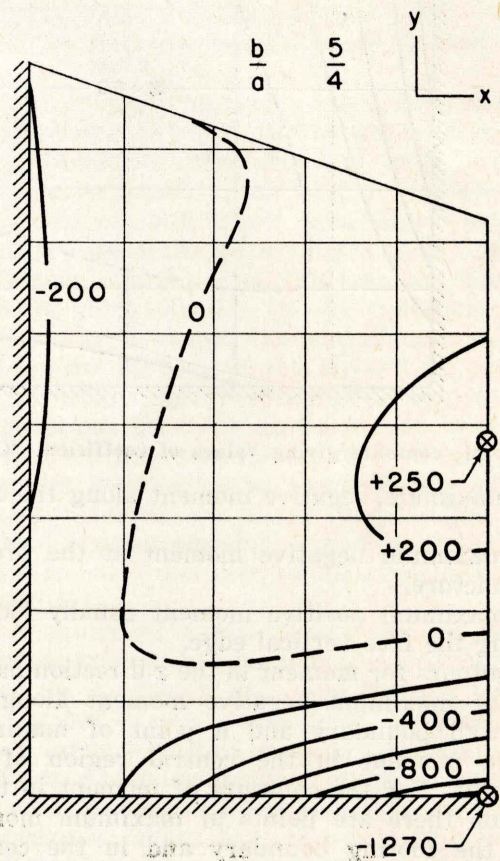
Fig. 22. M_y contours giving values of coefficient "C".

12

Fig. 23. M_x contours giving values of coefficient "C".
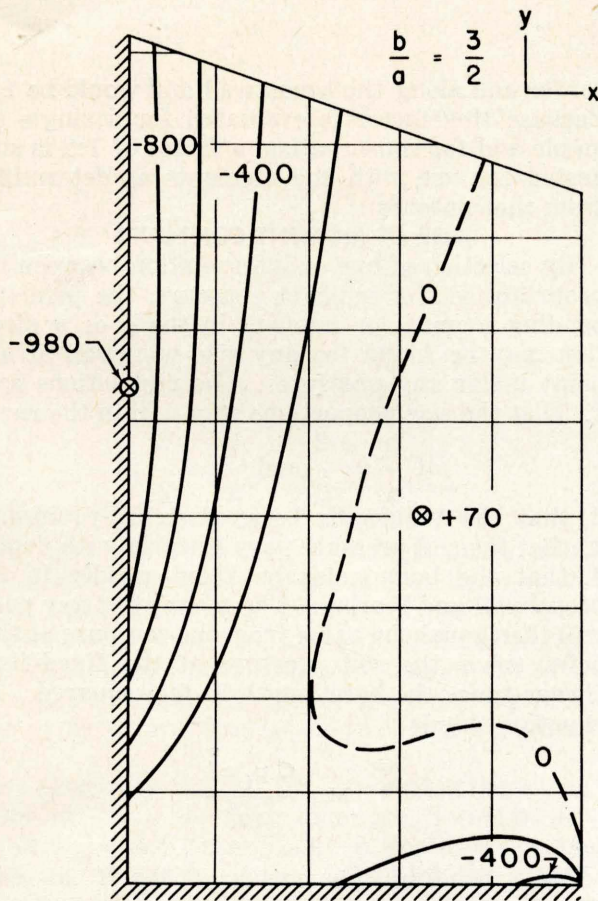
Fig. 24. M_y contours giving values of coefficient "C".

The moment changes due to the limiting parameter of considering the base hinged (complete freedom of rotation) was investigated for the wingwall of size ratio b/a = 1. A set of finite difference equations was written considering this boundary hinged, i.e., normal moment zero, with remaining boundaries staying the same. The equations were solved, and the moments were evaluated as shown earlier. Principal moment contours were drawn (figure 25). A comparison of the fixed-hinged contours with the contours drawn for the assumed fixed-fixed boundary of the wingwall No. 3 (figure 9) will indicate a moment increase of roughly twice the values of the fixed-fixed contours in the central and breastwall boundary region of the wingwall. A suggested safety factor of two for the central and breastwall boundary moments would be highly conservative, for the wingwall does not have complete freedom of rotation. It is built rigidly to the footing and the footing exercises considerable restraint to this boundary because of its own structural rigidity as well as that afforded by the soil, rock, or pile foundation.

A comparison between the slope at the footing boundary of a hinged wingwall and the rotation of a footing for a similar wingwall when connected monolithically to the footing was desirable as a means of determining the moment change. The
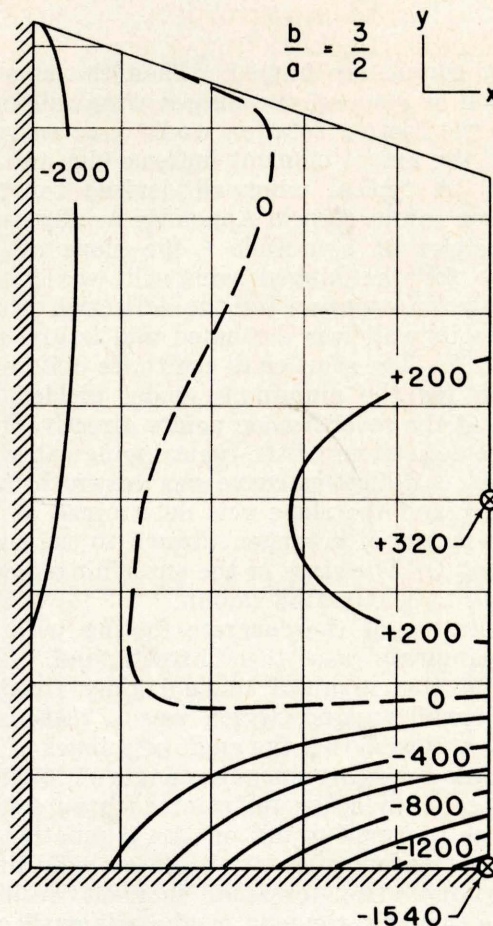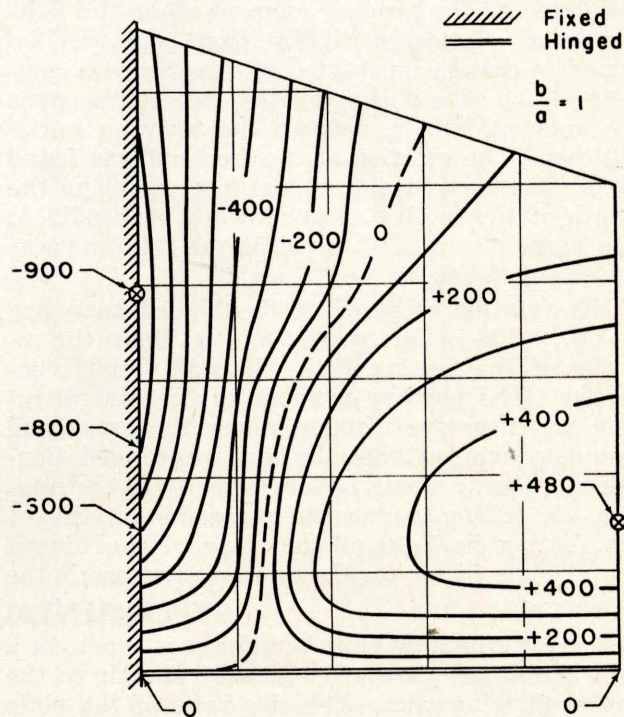
Fig. 25. Maximum principal moment contours of coefficient "C" for hinged footing boundary.

bending moments have been evaluated by finite differences for lower boundary walls with complete fixity (no rotation) and also with a lower

13

boundary completely hinged. Then the amount of rotation or slope of the hinged wingwall compared to the footing rotation would give an indication of the actual moment increase due to that rotation. A typical wingwall devised for this comparison can be seen in Appendix A. By using the principles of similitude [6] the slope of the boundary for the hinged wingwall was found. The prediction equation for the deflection of the concrete wingwall was evaluated and is given in Appendix A. The solution of the finite difference equations for the aluminum model yielded deflections at the several node points directly, from which the deflections of the typical wingwall were predicted. A deflection curve was drawn through the points, and the slope was determined at the hinge by means of a tangent drawn to the curve at that point. The slope at the outer hinged edge was found to be 0.000308 radian.

The rotation of the concrete footing with integral wingwall was then investigated. This foundation was assumed to be rigidly fixed to the breastwall footing, which was a reasonable assumption considering the angle of setback of the wingwall and the corresponding angle of juncture of footings. No other restraint such as soil or piling was assumed to act on the foundation; it was given freedom of rotation subject only to its own rigidity. The torsional moment resulted from the bending moment of the wingwall connected rigidly to the footing. This moment was calculated as the bending moment along the footing when considered rigidly fixed and was assumed to remain constant until rotation was complete which was a conservative procedure, since the moment will be reduced instantly on initial rotation. The rotation at the free end was found by integration of the torsional moment along the length of the footing as is shown in Appendix A. The angle of rotation found at the free end was 0.0000244 radian.

The rotation or slope of the hinged boundary was 0.000308 radian, more than ten times the rotation of the footing with wingwall rigidly connected. The positive moment in the central region and negative moment along the breastwall boundary doubled when the base was hinged. Considering the moments to vary directly as the rotation, and letting the maximum possible rotation of the footing be 1/10 of the slope of the hinged boundary, a factor for the moment increase in the center and along the breastwall and would be 1:1. Because this factor is evaluated for a single example and for conservatism a factor of 1:2 is suggested for use with the moments as determined from the contours.

USE OF MOMENT CONTOURS

By selection of one or interpolation between appropriate sets of moment contours, the principal bending moment or moment in the x or y direction may be found for any size wingwall at any point under any pressure. The restrictions are:
1. That the size proportions stay within the range of $\dfrac{b}{a} = \dfrac{2}{3}$ and $\dfrac{b}{a} = \dfrac{3}{2}$;
2. that the wingwalls be geometrically similar;
3. that the soil pressure vary linearly with depth;
4. that the boundaries be fixed rigidly to the breastwall and footing. The moment at any point will then equal the value from the contours at that point times the soil pressure at the fixed-fixed corner times the base length in feet squared. By equation this is

$$M = \frac{C\, p_f\, a^2}{10^4}$$

where:
  M = bending moment in ft-lbs/ft of edge length
  C = coefficient from moment contours
  p_f = normal soil pressure at the fixed-fixed corner in psf
  a = wingwall base length in feet.

Since rotation of the footing is possible, the factor of 1.2 is suggested for use in calculating positive moments in the central region and negative moments adjacent to the breastwall juncture. The moment equation will then be

$$M = \frac{1.2\, C\, p_f\, a^2}{10^4}$$

It can be noted that p_f and a^2 are constants for any given wingwall. The moment expression can then be written $M = K\,C$ and $M = 1.2\,K\,C$ in which K is $(p_f\, a^2)/10^4$. The directions of the maximum principal moments may be found from the appropriate moment trajectories. The dashed trajectory indicates compression on the back face; the solid line indicates tension on that face. Moment calculations for a typical wingwall are shown in Appendix B.

EXPERIMENTAL INVESTIGATION

The experimental investigation was made on a thin aluminum plate geometrically similar to the abutment wingwalls. The size ratio of the plate was $\dfrac{b}{a} = \dfrac{5}{4}$. It was concluded that a verification of the finite difference theory by experimental tests on a plate of this proportion along with the previously conducted tests on one of size ratio $\dfrac{b}{a} = \dfrac{4}{5}$ would give substantial evidence of accuracy of the equations. (For a comparison of the sizes see figure 2.) These tests would enable the safe use of the finite difference equations for application to the five wingwall proportions being investigated.

14
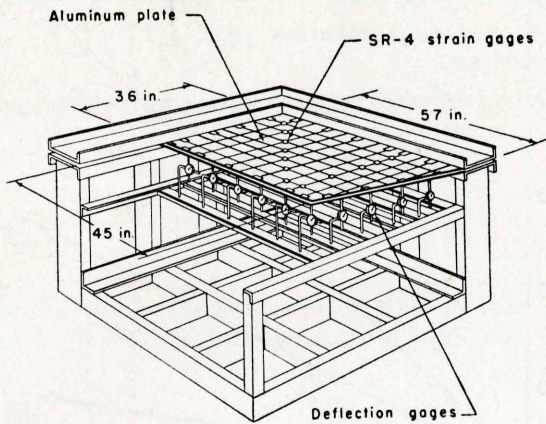
Fig. 26. Diagram of test plate in support frame.

The ½ x 36 x 45 inch aluminum plate was grouted and then bolted between the channels of a rigid steel framework that furnished the assumed boundary conditions of two adjacent edges fixed. A diagram of the support framework and plate can be seen in figure 26, and a photograph of the experimental test set-up is shown in figure 28.

The plate was gaged for measuring bending strains in the following manner. Twenty-two pairs of Type A-5 linear Baldwin electrical strain gages were placed in regions for which the direction of principal strain was shown. Twelve pairs
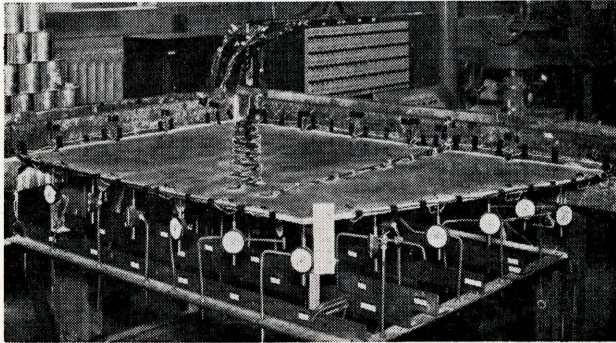
Fig. 28. Experimental plate before loading showing location of strain gages.

of Type AR-1 rosette gages were placed along the lines corresponding with lines of the grid system for which the finite difference equations were written (figures 27 and 28). This arrangement allowed a comparison of theoretical and experimental results by means of moment curves along the gage lines. The electrical strain gages were placed on both sides of the plate with the gages on one side in line with the corresponding gages on the opposite side of the plate. Each pair of gages acted as a single unit but with twice the sensitivity of a single gage. The gages were wired through a switchboard to the opposite sides of the wheatstone bridge in the Type M Baldwin Southwark measuring unit. As the plate was deflected normal to its middle plane, bending strains were introduced. The resistance of the gage on the tension side increased while the other in com-
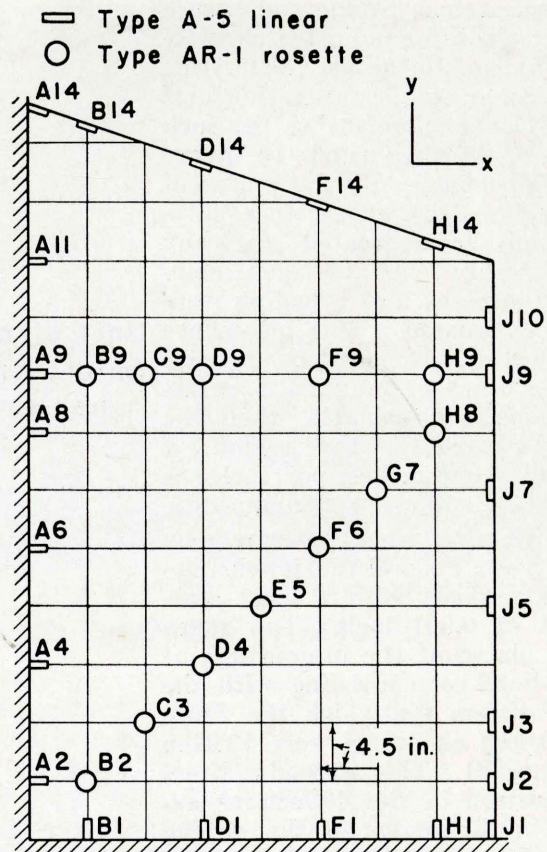
Fig. 27. Location of SR-4 strain gages.
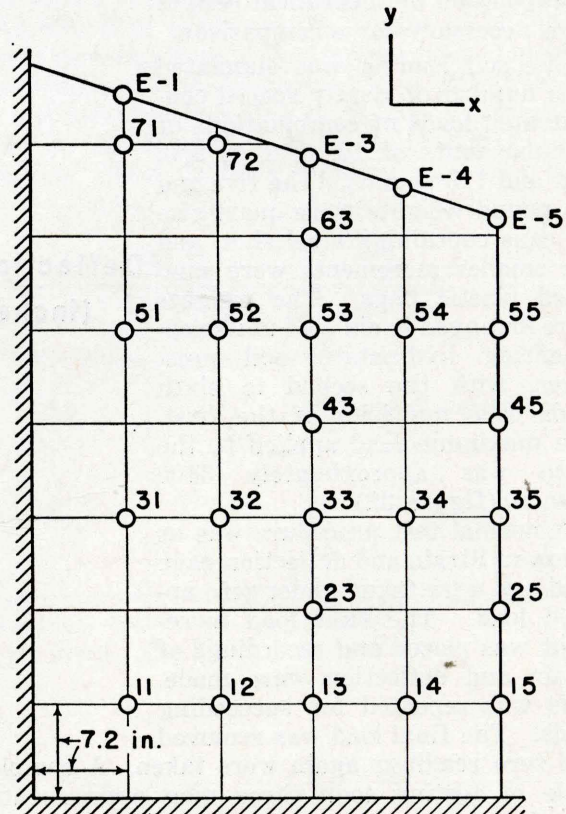
Fig. 29. Location of deflection gages.

pression decreased its resistance. This combination had a multiplying effect on the balance of

the wheatstone bridge and caused the strain to be indicated as twice the value of the actual strain. The least count on the measuring unit was then 5 micro inches per inch instead of the usual 10 micro inches per inch. By this means of connection, the gages were automatically compensated for any temperature changes, and membrane stresses under loading were also eliminated. This procedure was believed to greatly increase the accuracy of the results, a factor especially valuable when the strains were in the region of 0–1000 micro-inches per inch, as was true in these particular tests.

Deflections were measured by twenty-six Federal full jeweled deflection gages with a least scale count of 0.001 inch. The gages were placed at the intersection of grid lines corresponding with the grid system for which the finite difference equations were written (figure 29). This allowed a direct comparison of the deflections except in the region of the sloping edge for which interpolation and extrapolation of theoretical results were necessary for a comparison.

The soil loading was simulated by a number of closely spaced concentrated loads of combinations of modular units of 10, 5, 2, 1, 2/3, 1/2, and 1/3 pounds. The five and ten pound weights were quart size tin cans containing steel shot, and the smaller increments were sand filled plastic bags. The weights were arranged in six load units representing hydrostatic soil pressures, with the second to sixth loads each multiples of the first. The maximum load applied to the plate was approximately 3100 pounds (figure 32).

A normal test procedure was as follows: Strain and deflection gage readings were taken under zero applied load. The first load increment was placed and recordings of strain and deflection were made. This was repeated for succeeding loads. The final load was removed and zero readings again were taken. A complete cycle of testing took three men approximately four hours time.

Load-strain and load-deflection curves were plotted for all recorded data (figures 30 and 31).
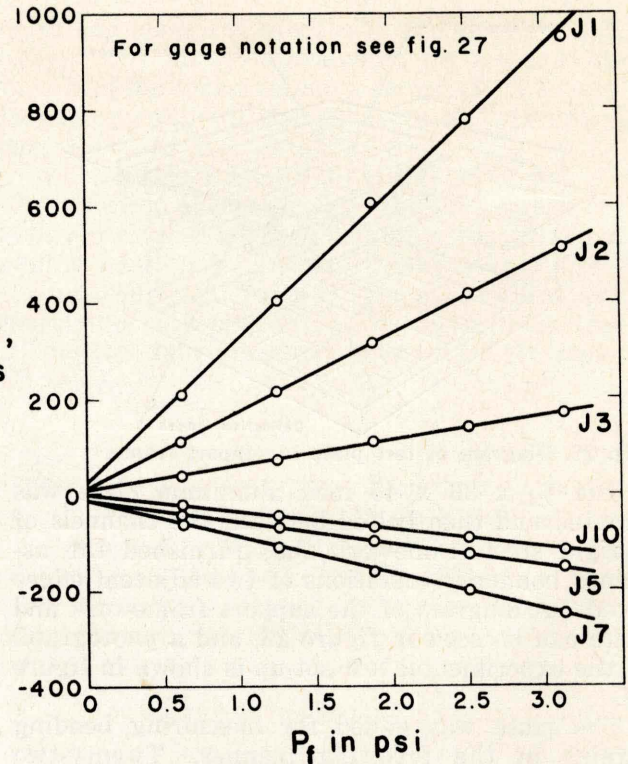
Fig. 30. Typical load-strain curves.
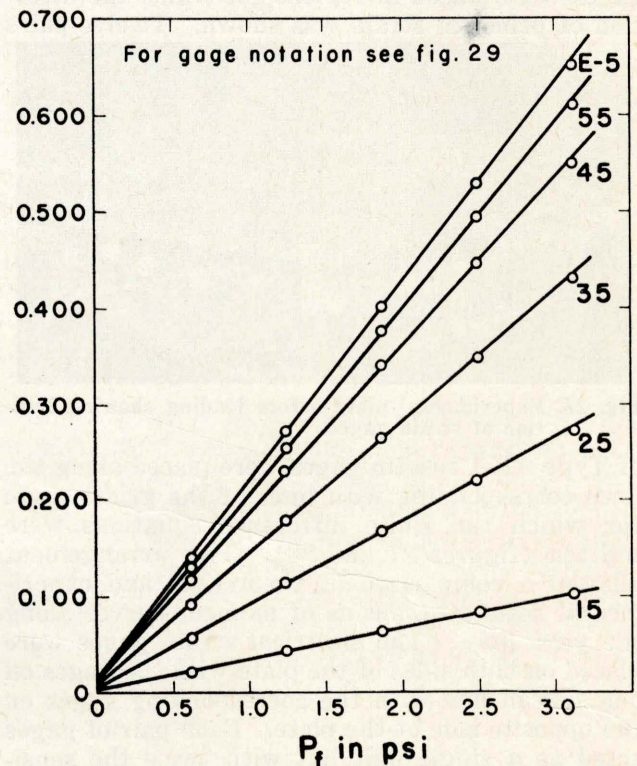
Fig. 31. Typical load-deflection curves.

The slopes were determined, and the strain and deflection ordinates were found for a pressure of 1 psi at the fixed-fixed corner. The pressure of 1 psi was the standard for all experimental-theoretical comparisons made.

Principal strains and directions of principal strains from the rosettes were obtained graphically. Stresses were evaluated by the formulas for two dimensional plane stress systems [5, 13],

$$\sigma_u = \frac{E}{1 - \mu^2} (e_u + \mu\, e_v)$$

$$\sigma_v = \frac{E}{1 - \mu^2} (e_v + \mu\, e_u)$$

And bending moment considering a unit edge length of plate was found by the equation[1]

$$M = \frac{\sigma h^2}{6}$$

which results directly from the common expression for moment of

$$M = \frac{\sigma I}{h/2}$$
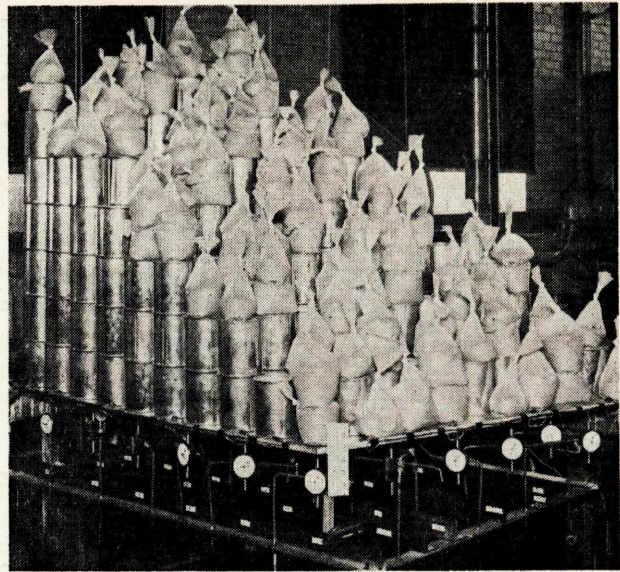
Fig. 32. Experimental plate under maximum load.

COMPARISON OF EXPERIMENTAL AND THEORETICAL RESULTS

Comparisons between theoretical and experimental moments are made along several gage lines (figures 33 to 35). All experimental-theoretical comparisons are made for a distributed pressure at the fixed-fixed corner of 1 psi and a base length of 36 inches. The moment curves along the lines A-B and E-F (figures 33 and 34) are for normal moments along the fixed boundaries. It can be noted that the moments determined experimentally are slightly less than those found theoretically. Since it is impossible to attain an absolutely rigid fixed support, the resulting rotation along the edges would cause this moment reduction provided that rotation of both boundaries were approxi-

mately the same. If one boundary rotated, however, while the other remained rigidly fixed, there would be a moment increase along the latter due to rotation of the adjacent boundary. Since the two supports on the experimental frame had approximately the same torsional rigidity, it can be safely assumed that the small inevitable rotations were about the same for each.

As discussed earlier in the section on the theoretical investigation, a twisting moment along the free boundary was determined from the theoretical analysis and was due to certain assumptions made in the derivation of the differential plate equation. This twisting moment was used with
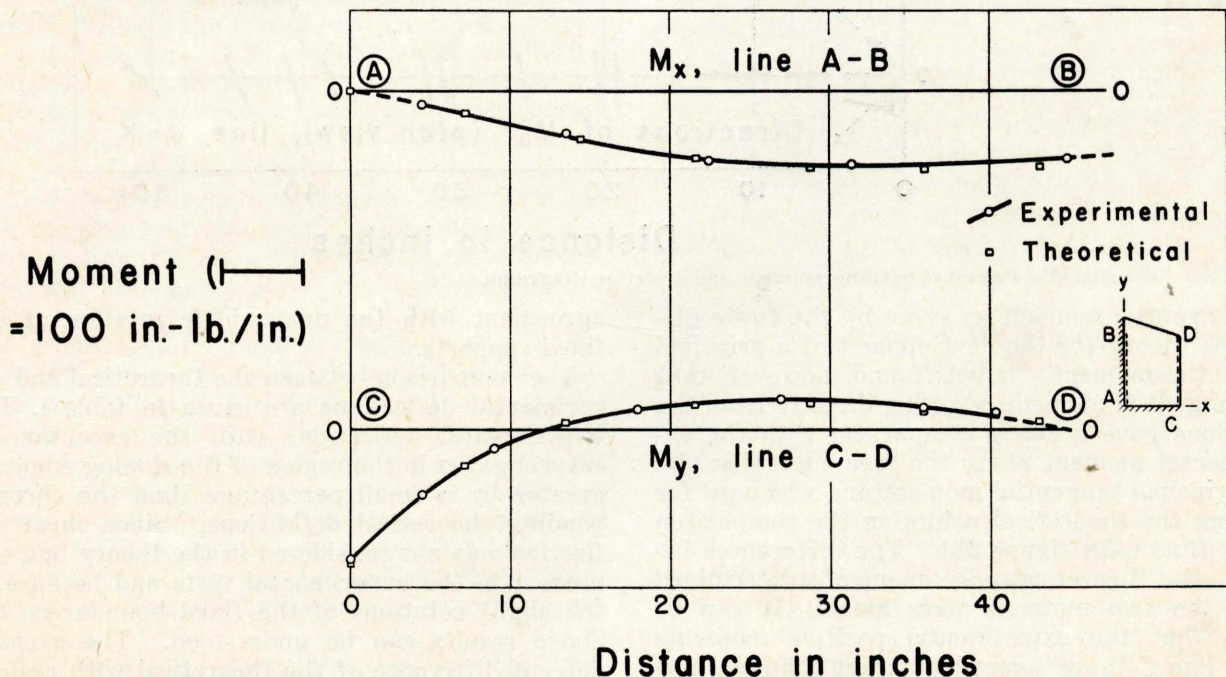
Fig. 33. Bending moment diagrams.
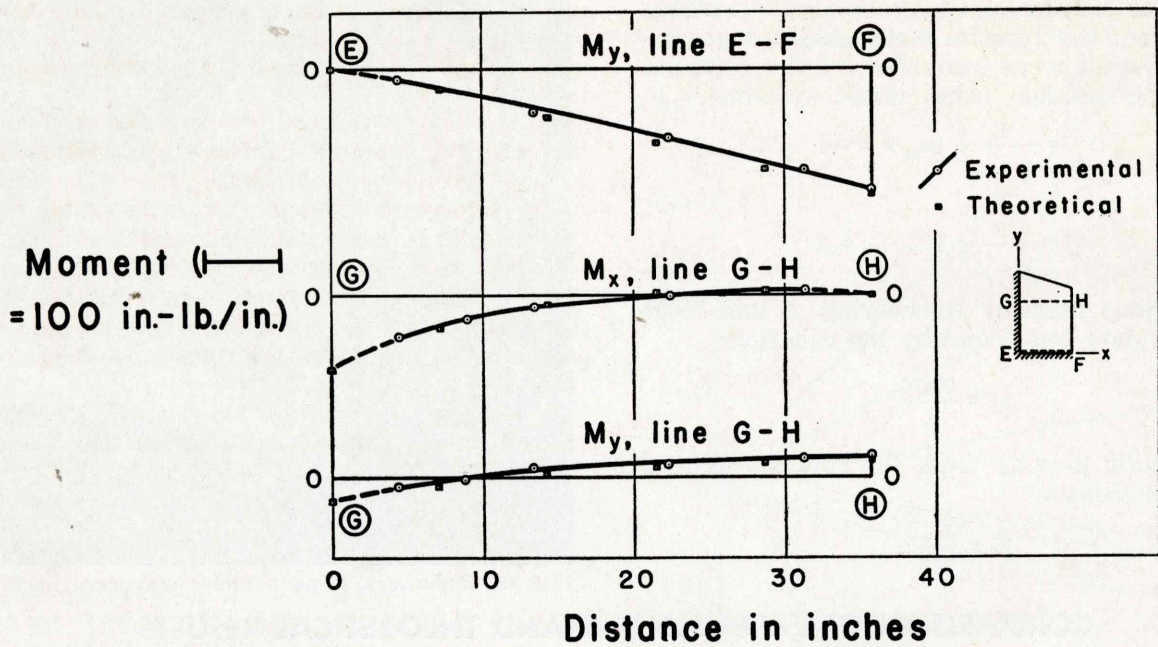
Fig. 34. Bending moment diagrams.
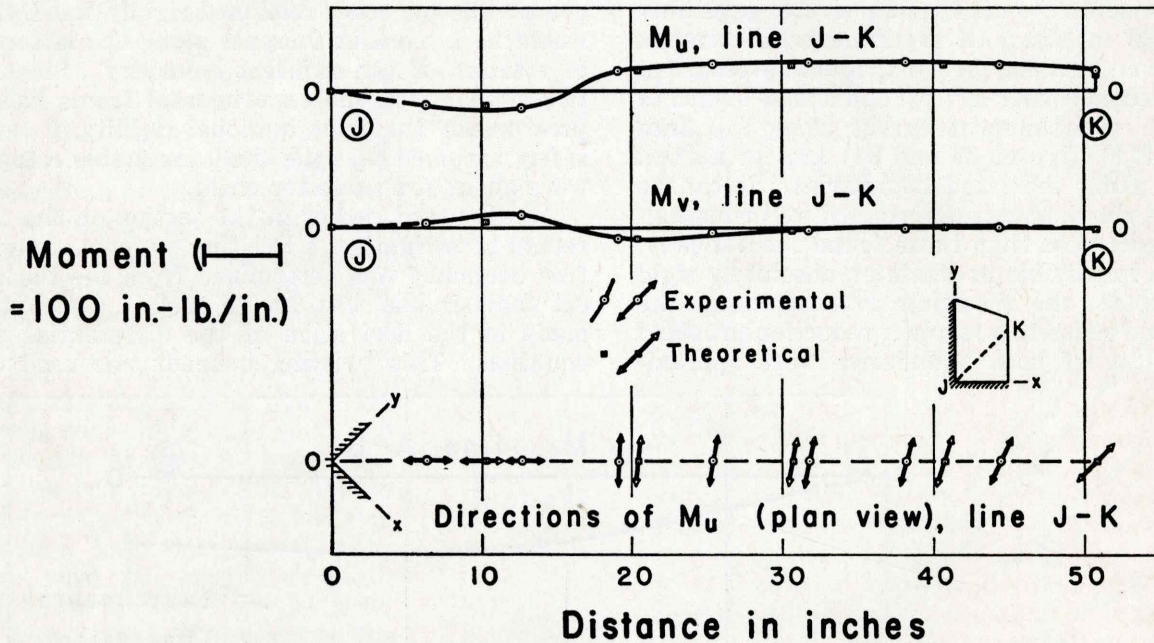
Fig. 35. Principal bending moment and direction diagrams.

the tangential moment as given by the finite difference theory for the development of a principal tangential moment. It was found, however, that the tangential moment resulting directly from the equations gave a closer comparison with the experimental moment along the free edge than did the principal tangential moment and was used for plotting the theoretical points on the comparison curve (line C-D, figure 33). The differences between the theoretical edge moments determined from the two methods were small. It can be noted that the experimental positive moments along line C-D are somewhat larger than the corresponding theoretical moments which is an

agreement with the unavoidable rotation of the fixed supports.

The comparison between the theoretical and experimental deflections are given in table I. The experimental deflections with the exception of several gages in the region of the sloping edge are greater by a small percentage than the corresponding theoretical deflections. Since shear deflection was not considered in the theory but was present in the experimental tests and because of the slight rotations of the fixed boundaries, the above results can be understood. The average percent difference of the theoretical with respect to the experimental deflections was ± 3.9%.

Table I. Comparison between experimental and theoretical deflections.

Gage* No.	Test No. 1 Exp. w (in.)	Test No. 2 Exp. w (in.)	Average Exp. w (in.)	Theoretical w (in.)	Percent Difference with Exp.
11	0.006	0.006	0.006	0.006	0.0%
12	.014	.014	.014	.013	7.1
13	.021	.020	.020	.020	0.0
14	.028	.027	.027	.027	0.0
15	.034	.034	.034	.033	2.9
23	.051	.051	.051	.051	0.0
25	.088	.088	.088	.087	1.1
31	.019	.020	.019	.017	10.5
32	.047	.049	.048	.046	4.2
33	.077	.077	.077	.077	0.0
34	.109	.108	.108	.107	0.9
35	.141	.140	.140	.136	2.9
43	.098	.097	.097	.094	3.1
45	.179	.178	.178	.172	3.5
51	.023	.024	.023	.020	13.0
52	.061	.062	.061	.059	3.3
53	.105	.105	.105	.104	1.0
54	.153	.153	.153	.148	3.3
55	.199	.200	.199	.193	3.0
63	.109	.107	.108	.107	0.9
71	.017	.017	.017	.018	-5.9
72	.053	.054	.053	.059	-11.3
E-1	.015	.013	.014	.016	-14.3
E-3	.106	.106	.106	.109	-2.8
E-4	.162	.161	.161	.159	1.2
E-5	.212	.210	.211	.207	1.9

*For gage notation see figure 29

A conclusive verification of the finite difference theory was made [3] on a wingwall model of size ratio $\dfrac{b}{a} = \dfrac{4}{5}$. A portion of the strain gage data from the tests was used to check the accuracy of the principal moment contours for that particular size proportion. Principal moments and directions corresponding to a pressure at the fixed-fixed corner of 3 psi (432 psf) and base length of 3.75 feet were evaluated for several points on the plate. Principal moments were predicted from the contours for the pressure of 432 psf and base length of 3.75 feet, and the comparison is given in table II.

Table II. Comparison between experimental and theoretical moments calculated from contours.

b/a = 4/5
a = 3.75 ft
p_f = 432 psf

$$M = \frac{C\, p_f\, a^2}{10^4}$$

Coordinate* x (ft.)	y (ft.)	Experimental M_u (ft-lb/ft)	θ_x	Theoretical M_u (ft-lb/ft)	θ_x	Percent Difference of Moment with Experimental
3.00	0.37	-181	85	-207	77	14.4%
3.75	0.00	-455	—	-438	90	-3.7
2.25	2.25	97	-52	82	-49	-15.5
0.37	2.25	-137	7	-146	6	6.6
0.00	3.00	-254	—	-275	0	8.3
3.00	2.25	81	-57	85	-52	4.9

*See figure 17 for direction of coordinates. The location of the origin is at the fixed-fixed corner.

DISCUSSION

During the process of this investigation several items influenced the accuracy of the finite difference equations and the resulting moment contours:

1. Simplification of the sloping edge—To write the finite difference conveniently the sloping edge of the wingwall was replaced by a horizontal edge passing through the approximate mid-point of the original boundary. The experimental results indicate that this simplification had little effect on deflections and moments in the major portion of the wingwall.

2. Size of grid spacings — The accuracy of the finite difference equations depended largely on the grid spacing and the resulting number of equations written. The use of 30-40 linear simultaneous equations for each plate [3] gave satisfactory results.

3. Value used for Poisson's ratio — A Poisson's ratio of 0.3 was used in all finite difference equations for deflection and moment. The equations are not independent of the ratio; however, it is believed that the use of a Poisson's ratio of 0.3 instead of, say, 0.2 a more common value for concrete, had only a small effect on the resulting moments. Any discrepancies resulting from this difference are believed to be less than those caused by other assumptions used in the method, 1, p. 15.

4. Sensitivity of moment equations—The bending moments by finite difference theory were functions of the differences of deflections of near equal magnitude. The use of at least five or preferably six significant figures for the deflections will give results for the moment of stresses comparable with the over-all accuracy of the numerical method.

The experimental tests were also affected by several factors which are given below:

1. Fixation of edges — It is impossible to attain experimentally an edge absolutely fixed against rotation. However, the steel framework used in the experimental tests produced as good a fixed support as might be attained.

2. Approximation of load — A series of free standing weights closely approached the hydrostatic type of loading which is normally assumed for soil pressures.

3. Use of electrical strain gages — The bending strains were measured at a point by two strain gages, one located on each side of the plate. The two gages acted as a double indicating unit and measured the bending strains more accurately than by a single gage.

4. Shear deflection — Shear deflection was not considered in the theoretical calculation but was present in the experimental tests. These deflections could not be separated from those due to bending, but it is believed the shear deflections contributed only a small percentage to the total deflections of the plate.

19

SUMMARY AND CONCLUSIONS

This investigation consisted of several sections which are listed with their conclusions as follows:

1. Further experimental verification of the finite difference numerical method was made by tests on a wingwall model of a different size proportion than that investigated in part two of the project. This investigation gave substantial evidence to the accuracy and reliability of the numerical method.

2. The development of bending moment contours by use of the finite difference method was made which enables the calculation of moment at any point in the wingwalls. Contours were developed for maximum principal bending moment and for moments in the x and y directions. The directions of the maximum principal moments were found and presented in the form of moment trajectories. The equation for the moment calculation to be used in connection with the contours is given as

$$M = \frac{C\,p_f\,a^2}{10^4}$$

where

C = coefficient from the moment contours
p_f = normal soil pressure at the fixed-fixed corner in psf
a = base length of wingwall in feet

The accuracy of the bending moments determined from the contours is approximately $\pm$ 8% along the fixed boundaries and $\pm$ 15% in the central region where the error, though large in percentage, is small in magnitude.

3. An investigation was made of the footing rotation with its resulting effects on the moments in the wingwall. It was concluded that a factor of 1.2 to be used in the previously mentioned moment equation was satisfactory to cover the moment increase along the breastwall boundary and in the central region of the wingwall. The equation for these moments will be

$$M = \frac{1.2\,C\,p_f\,a^2}{10^4}$$

SELECTED REFERENCES

1. Barton, M. V. Finite Difference Equations for the Analysis of Thin Rectangular Plates with Combinations of Fixed and Free Edges. CF-1005, DRL-175, Defense Research Laboratory. University of Texas, Austin, Texas. August 6, 1949. (Mimeo.)

2. Chettoe, C. S. and Adams, H. C. Reinforced Concrete Bridge Design. 2nd ed. Chapman and Hall. London. 1938.

3. Harrenstien, H. P. and Alsmeyer, W. C. Structural Behavior of a Plate Resembling a Constant Thickness Bridge Abutment Wingwall. Bulletin 182. Iowa Engineering Experiment Station. Ames, Iowa. 1959.

4. Hool, G. A. and Johnson, N. C. Concrete Engineer's Handbook. McGraw-Hill Book Co. N. Y. 1918.

5. Lee, G. H. An Introduction to Experimental Stress Analysis. John Wiley and Sons. N. Y. 1950.

6. Murphy, G. Similitude in Engineering. Ronald Press Co. N. Y. 1950.

7. Parcel, J. I. and Moorman, R. B. B. Analysis of Statistically Indeterminate Structures. John Wiley and Sons. N. Y. 1955.

8. Portand Cement Association. Concrete Bridge Details. The Association. Chicago. 1942.

9. Southwell, R. V. An Introduction to the Theory of Elasticity. 2nd ed. Oxford University Press. Oxford, England.

10. Southwell, R. V. Relaxation Methods in Theoretical Physics. Clarendon Press. Oxford, England. 1946.

11. Taylor, F. W., Thompson, S. E. and Smulski, E. Reinforced Concrete Bridges. John Wiley and Sons. N. Y. 1939.

12. Timoshenko, S. Theory of Plates and Shells. McGraw-Hill Book Co. N. Y. 1940.

13. Wang, Chi-teh. Applied Elasticity. McGraw-Hill Book Co. N. Y. 1953.

The analysis for deflections and resulting slope of the hinged boundary and rotation of the footing was made on a typical concrete wingwall which is shown in figure 36.

Front view

End view
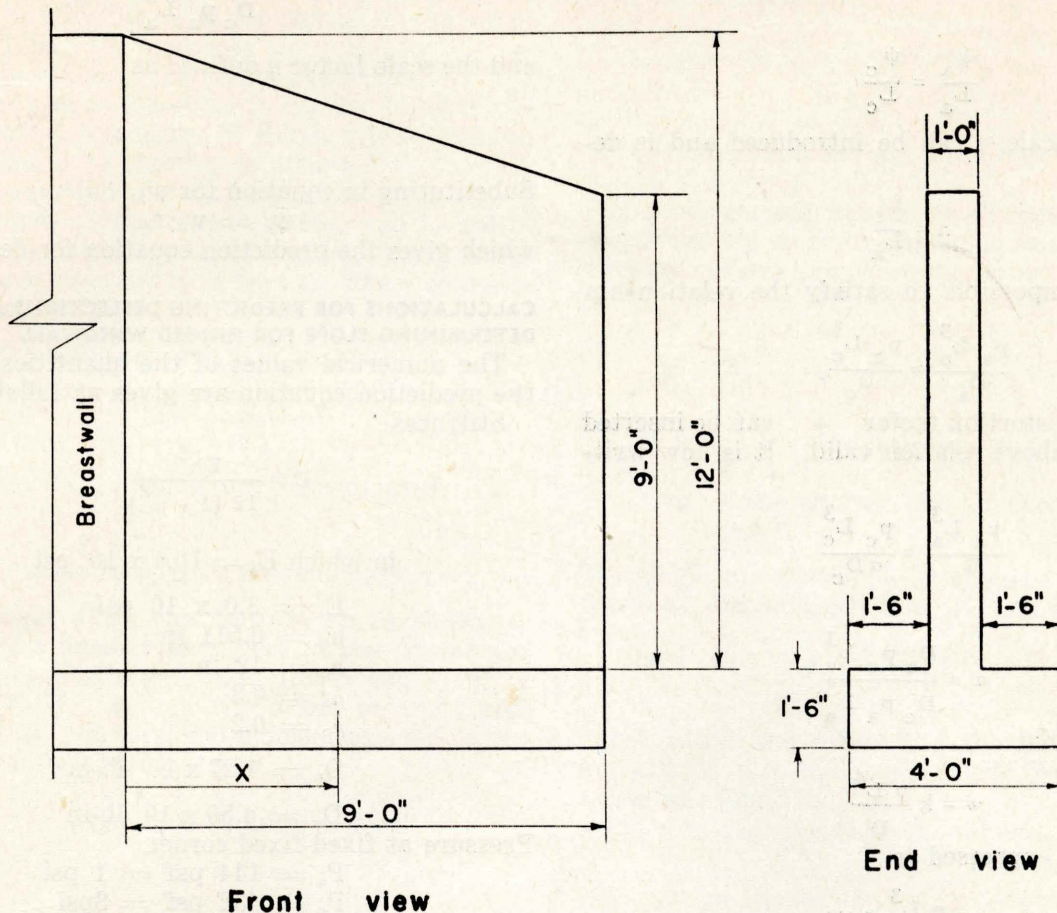
Fig. 36. Concrete wingwall for slope and footing rotation analysis.

PREDICTION EQUATION FOR WINGWALL DEFLECTIONS

The deflection of a geometrically similar wingwall may be predicted from the known deflection of another wingwall by use of the principles of similitude.[6]

The deflection of a given plate under distributed loading at any point can be expressed as

$$w = k \frac{p L^4}{D}$$

where

$$D = \frac{E h^3}{12 (1 - \mu^2)}$$

$$k = \text{a dimensionless constant}$$

The variables involved and the basic dimensions in which they can be expressed are given as

Variable	Definition	Dimension
w	Deflection	L
p	Distributed load	$P L^{-2}$
D	Plate stiffness	$P L$
L	A specific length	L
ψ	Any length	L

The number of required dimensionless and independent terms (Pi terms) to express a relationship between the variables is indicated by the Buckingham Pi Theorem which states

$$s = n - g$$

where

s = number of dimensionless Pi terms required.

n = number of variables involved

g = number of basic dimensions used to describe the variables

s = 5 − 2 = 3 Pi terms required

The three dimensionless Pi terms may be written as

$$\left(\frac{w}{L}\right), \left(\frac{\psi}{L}\right), \left(\frac{p L^3}{D}\right)$$

The Pi term involving deflection, the quantity which is desired, can be expressed as a function of the remaining terms, thus

$$\frac{w}{L} = f\left(\frac{\psi}{L}, \frac{p L^3}{D}\right)$$

Letting the subscript a designate quantities for the aluminum model and the subscript c designate those for the concrete wingwall the above equation can be written

21

$$\frac{w_a}{L_a} = f\left(\frac{\psi_a}{L_a}, \frac{p_a L_a^3}{D_a}\right) \text{ and } \frac{w_c}{L_c} = f\left(\frac{\psi_c}{L_c}, \frac{p_c L_c^3}{D_c}\right)$$

Let

$$\frac{\psi_a}{L_a} = \frac{\psi_c}{L_c}$$

The length scale n can be introduced and is defined as

$$n = \frac{L_c}{L_a}$$

It may be impossible to satisfy the relationship

$$\frac{p_a L_a^3}{D_a} = \frac{p_c L_c^3}{D_c}$$

However, a distortion factor α can be inserted making the above relation valid. It is now written

$$\frac{p_a L_a^3}{D_a} = \frac{p_c L_c^3}{\alpha D_c}$$

with

$$\alpha = \frac{D_a p_c L_c^3}{D_c p_a L_a^3}$$

It is known that

$$w = k \frac{p L^4}{D}$$

which can be expressed as

$$w = \frac{p L^3}{D} f(\psi)$$

Dividing by L,

$$\frac{w}{L} = \frac{p L^3}{D} f\left(\frac{\psi}{L}\right)$$

This can be written as

$$\frac{w_a}{L_a} = \frac{p_a L_a^3}{D_a} f\left(\frac{\psi_a}{L_a}\right) \text{ and } \frac{w_c}{L_c} = \frac{p_c L_c^3}{D_c} f\left(\frac{\psi_c}{L_c}\right)$$

Dividing the latter by the first,

$$\frac{\frac{w_c}{L_c}}{\frac{w_a}{L_a}} = \frac{\frac{p_c L_c^3}{D_c} f\left(\frac{\psi_c}{L_c}\right)}{\frac{p_a L_a^3}{D_a} f\left(\frac{\psi_a}{L_a}\right)}$$

Since $\dfrac{\psi_a}{L_a} = \dfrac{\psi_c}{L_c}$ the last terms cancel and solving for w_c we get

$$w_c = w_a \left(\frac{L_c}{L_a}\right)\left(\frac{D_a}{D_c}\right)\left(\frac{p_c}{p_a}\right)\left(\frac{L_c^3}{L_a^3}\right)$$

The distortion factor α has been defined as

$$\alpha = \frac{D_a p_c L_c^3}{D_c p_a L_a^3}$$

and the scale factor n defined as

$$n = \frac{L_c}{L_a}$$

Substituting in equation for w_c,

$$w_c = w_a n \alpha$$

which gives the prediction equation for deflection.

CALCULATIONS FOR PREDICTING DEFLECTIONS AND DETERMINING SLOPE FOR HINGED WINGWALL

The numerical values of the quantities used in the prediction equation are given as follows:

Stiffness

$$D = \frac{Eh^3}{12(1 - \mu^2)}$$

in which $E_a = 10.4 \times 10^6$ psi

$E_c = 3.0 \times 10^6$ psi

$h_a = 0.511$ in

$h_c = 12$ in

$\mu_a = 0.3$

$\mu_c = 0.2$

$D_a = 1.27 \times 10^5$ lb-in

$D_c = 4.50 \times 10^8$ lb-in

Pressure at fixed-fixed corner

$P_a = 144$ psf $= 1$ psi

$P_c = 432$ psf $= 3$ psi

Scale and distortion factors

$n = L_c/L_a = 3$

$\alpha = \dfrac{D_a}{D_c} \dfrac{p_c}{p_a} n^3 = 2.29 \times 10^{-2}$

The prediction equation can be expressed as

$$w_c = w_a n \alpha = w_a (0.0687)$$

The deflection at the several node points along the vertical free edge were obtained directly from the solution of the finite difference equations for the aluminum model, and the deflections for the concrete wingwall were predicted by the above equation.

Table III. Predicted deflections along vertical free edge.

Grid No.	Distance from footing		Deflection	
	d_a	d_c	w_a	w_c
	(in)	(in)	(in)	(in)
05	0.	0.	0.	0.
15	7.2	21.6	0.0865	0.0059
25	14.4	43.2	0.1549	0.0106
35	21.6	64.8	0.2002	0.0138
45	28.8	86.4	0.2257	0.0155

A deflection curve along the vertical edge was plotted and the slope at the hinged footing determined from a tangent drawn to the curve at that point. The slope was found to be

$$\phi = 3.08 \times 10^{-4} \text{ radians}$$

ROTATION OF FOOTING WITH MONOLITHIC WINGWALL

The assumptions for the footing rotation analysis are as follows:

1. Torsional moments are introduced into the footing by the rigid connection of the wingwall, and the moments along the footing remain constant throughout rotation.
2. The wingwall footing is rigidly fixed to the breastwall footing; no soil or pile foundation restraint to rotation is afforded throughout the remainder of its length.

The moment at the outside corner can be calculated by use of the moment contours for a wingwall of size ratio $b/a = 9/9 = 1$. These contours are shown in figure 9.

The equation for moment is

$$M = \frac{C \, p_f \, a^2}{10^4}$$

in which C = 960 (from the contours)
p_f = 432 psf
a = 9 ft
M = 3360 ft-lb/ft at the outside corner.

The moment along the footing can be shown to vary almost linearly from zero at the fixed-fixed corner to a maximum value at the edge (figure 34, line E-F). Taking the origin at the fixed-fixed corner, the torsional moment exerted on the footing can be expressed as

$$T = 374 \, (x)$$

where x is in units of feet.

The modulus of rigidity for concrete was found by the expression [13],

$$G_c = \frac{E_c}{2 \, (1 - \mu_c)}$$

in which $E_c = 3 \times 10^6$ psi

$$\mu_c = 0.2$$

$$G_c = 1.25 \times 10^6 \text{ psi} = 180 \times 10^6 \text{ psf}$$

For a rectangular section the torsional constant corresponding to the polar moment of inertia for circular sections can be expressed as [7]

$$J = \frac{t \, m^3}{16} \left[\frac{16}{3} - 3.36 \frac{m}{t} \left(1 - \frac{m^4}{12 \, t^4} \right) \right]$$

in which t = the longer side of the rectangle = 4 ft
m = the shorter side of the rectangle = 1.5 ft

The angle of rotation ϕ at the end can now be found by the integration of the expression,

$$\phi = \int_0^L \frac{T \, dx}{G \, J}$$

Substituting and evaluating the integral for an upper limit of 9, the length of the footing, the rotation was found to be

$$\phi = 2.44 \times 10^{-5} \text{ radians}$$

APPENDIX B: EXAMPLE CALCULATIONS FOR BENDING MOMENT

A typical wingwall to illustrate the method of calculation of bending moments by use of the moment contours is shown in figure 37. From the figure it can be seen that $b = 12$ ft and $a = 15$ ft. The ratio b/a indicates that the contours for size proportion $b/a = 4/5$ are to be used. Principal moment contours for this size ratio are shown in figure 7, and contours for moments in the x and y directions are given in figures 17 and 18.
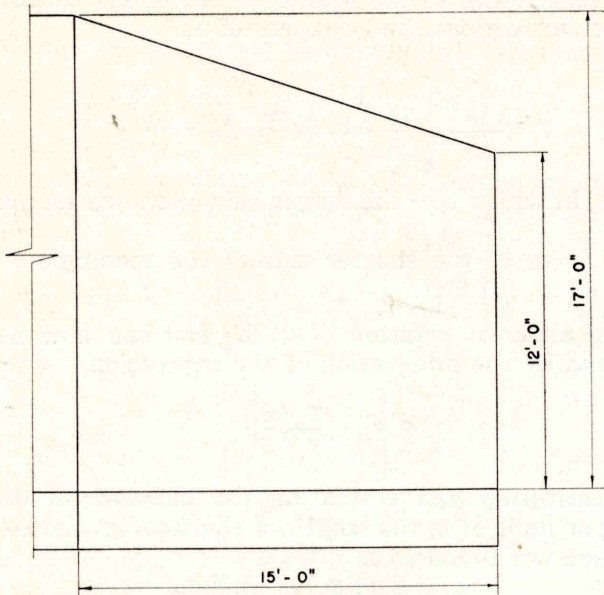
Fig. 37. Wingwall for example moment calculations.

Since it is common practice in a wingwall design to place the steel reinforcing horizontally and vertically the contours for moment in the x and y directions will be used to illustrate the moment calculations. However, the critical moments along the fixed boundaries and vertical free edge, all of which are in the x or y direction, can be found equally as well from the principal moment contours.

The equations for moment are

$$M = \frac{C \, p_f \, a^2}{10^4} \text{ (for negative moment along footing)}$$

and

$$M = 1.2 \frac{C \, p_f \, a^2}{10^4} \text{ (For all positive moments and}$$

negative moments along breast-wall)

in which $M =$ bending moment in ft-lb/ft

$C =$ coefficient from contours

$p_f =$ soil pressure at fixed-fixed corner in psf

$a =$ wingwall base length in feet

An equivalent hydrostatic soil pressure of 35 psf/ft will be used.

The pressure p_f at the fixed-fixed corner will then be

$$p_f = (35)(17.0) = 595 \text{ psf.}$$

The moments can now be expressed by

$$M = \frac{C \, (595) \, (15)^2}{10^4} = (13.4) \, C$$

The critical moment along the footing occurs at the outside edge. The coefficient for M_y at that point is $C = -720$. The bending moment will then be

$$M_y = (13.4)(-720) = -9640 \text{ ft-lb/ft.}$$

At the midpoint along the footing the coefficient C is -430. The moment at that point is

$$M_y = (13.4)(-430) = -5760 \text{ ft-lb/ft.}$$

The critical positive moment in the y direction occurs along the vertical free edge approximately 9 ft above the footing. The coefficient C is $+120$ and

$$M_y = (1.2)(13.4)(120) = 1930 \text{ ft-lb/ft.}$$

Along the breastwall juncture the critical region for moment in the x direction is near the top where $C = -460$.

$$M_x = (1.2)(13.4)(-460) = -7400 \text{ ft-lb/ft.}$$

The maximum positive moment in the x direction occurs about 9 ft horizontally from the breastwall and 8½ ft above the footing. At that point

$$M_x = (1.2)(13.4)(60) = 965 \text{ ft-lb/ft.}$$

APPENDIX C: TABULATION OF MOMENTS EVALUATED FROM FINITE DIFFERENCE EQUATIONS

The bending and twisting moments originally evaluated from the finite difference equations are tabulated for the five plate size ratios investigated and are shown in tables IV to VIII. The principal moments and direction of maximum principal moment determined from the above data are also included in the tables.

The original moments were evaluated for a plate base dimension of three feet and pressure at the fixed-fixed corner of 144 psf which corresponded to the dimensions and pressure of the experimental test plate. For use in determining the contours the moments were reduced for a wing-wall of unit base length of 1 ft and unit pressure at the fixed-fixed corner of 1 psf. This procedure is described in the section on the theoretical investigation.

Fig. 38. Typical grid notation.

Table IV. Moments in inch-pounds per inch for plate no. 1
b/a = 2/3
a = 3 ft
P_f = 144 psf

Grid* No.	M_x	M_y	M_{xy}	M_v	M_u	θ_x (Deg.)
01	-4.5	-15.1		-4.5	-15.1	90
02	-9.9	-33.1		-9.9	-33.1	90
03	-14.1	-46.9		-14.0	-46.9	90
04	-17.0	-56.5		-16.9	-56.5	90
05	-19.2	-64.0		-19.2	-64.0	90
06	-21.0	-70.1		-21.0	-70.1	90
10	-15.1	-4.5		-4.5	-15.1	0
11	-1.6	-0.9	-6.5	5.3	-7.8	44
12	0.8	-3.6	-7.1	6.0	-8.9	54
13	-0.7	-8.6	-5.8	2.4	-11.7	62
14	-3.1	-13.7	-4.5	-1.5	-15.3	70
15	-4.7	-17.6	-3.8	-3.6	-18.7	75
16		-20.2	-3.8		-20.9	90
20	-31.3	-9.4		-9.4	-31.3	0
21	-5.2	1.0	-6.4	5.4	-9.2	32
22	4.3	5.6	-8.2	-3.4	13.2	-47
23	6.0	6.3	-7.6	-1.6	13.8	-45
24	4.3	5.0	-6.3	-1.8	11.0	-47
25	1.7	3.3	-5.5	-3.1	8.1	-49
26		2.5	-7.0		8.4	90
30	-41.9	-12.6		-12.6	-41.9	0
31	-10.9	-1.5	-4.8	0.5	-12.9	23
32	3.3	5.1	-7.1	-3.0	11.3	-49
33	7.7	8.0	-7.3	0.5	15.2	-46
34	7.0	8.7	-6.4	1.4	14.3	-49
35	3.9	8.4	-5.4	0.4	14.0	-56
36		8.7	-5.1		11.1	90
40	-48.5	-14.6		-14.5	-48.5	0
41	-16.1	-3.9	-3.7	-2.9	-17.1	16
42	0.5	1.6	-6.1	-5.1	7.2	-47
43	7.0	4.1	-6.6	-1.2	12.3	-39
44	7.4	4.9	-5.7	0.3	12.1	-39
45	4.5	5.1	-4.3	0.5	9.1	-47
46		5.8	-3.0		7.1	90
50	-53.2	-16.0		-16.0	-53.2	0
51	-19.6		-3.4		-20.2	0
52	-1.6		-7.4		-8.3	0
53	6.3		-6.9		10.7	0
54	7.8		-5.3		10.5	0
55	5.3		-3.3		6.9	0

*See figure 38 for typical grid notation.

25

Table V. Moments in inch-pounds per inch for plate no. 2.
b/a = 4/5
a = 3 ft
p_f = 144 psf

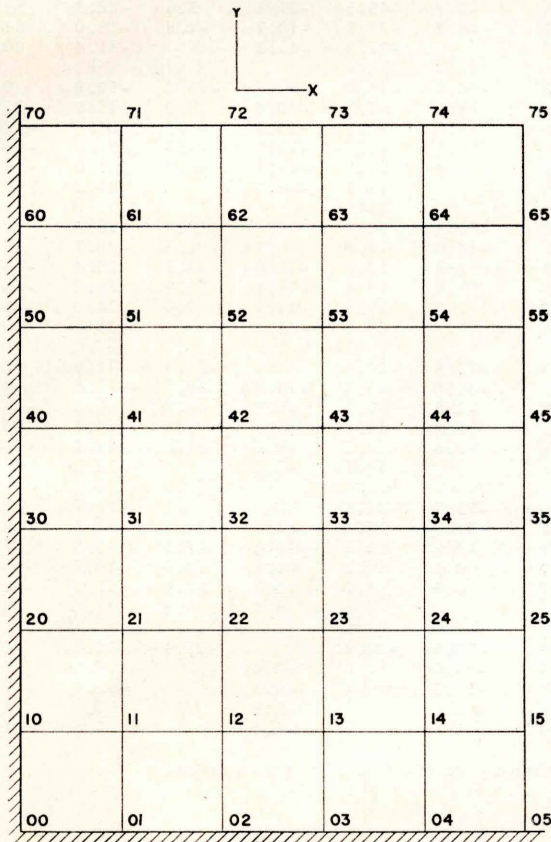| Grid* No.	M_x	M_y	M_{xy}	M_v	M_u	θ_x (Deg.)
01	-4.1	-13.7		-4.1	-13.7	90
02	-9.8	-32.5		-9.8	-32.5	90
03	-14.9	-49.2		-14.9	-49.2	90
04	-18.8	-62.6		-18.8	-62.6	90
05	-22.1	-73.8		-22.1	-73.8	90
06	-25.3	-84.4		-25.3	-84.4	90
07	-27.9	-93.0		-27.9	-93.0	90
10	-13.7	-4.1		-4.1	-13.7	0
11	-3.1	-2.7	-6.9	4.1	-9.9	44
12	-1.1	-6.9	-8.3	4.9	-12.9	55
13	-2.5	-13.5	-7.6	1.4	-17.4	64
14	-5.1	-20.4	-6.6	-2.7	-22.9	70
15	-7.8	-26.8	-5.8	-6.2	-28.5	74
16	-8.6	-31.8	-5.5	-7.4	-33.2	77
17		-35.6	-5.2		-36.4	90
20	-31.2	-9.4		-9.4	-31.2	0
21	-7.9	-0.5	-7.6	-0.3	-8.0	32
22	1.6	3.5	-10.3	-7.8	12.9	-48
23	4.1	3.8	-10.4	-6.5	14.4	-45
24	3.3	2.1	-9.5	-6.9	12.2	-43
25	1.1	-0.4	-8.5	-8.3	8.9	-42
26	-0.5	-2.7	-8.3	6.8	-10.0	49
27		-4.3	-11.2		-13.6	90
30	-44.5	-13.4		-13.4	-44.5	0
31	-14.5	-1.9	-6.0	0.5	-16.9	22
32	0.3	5.6	-9.1	-6.6	12.6	-52
33	6.3	9.7	-10.1	-2.3	18.3	-49
34	7.2	11.1	-9.7	-0.8	19.1	-51
35	5.7	11.2	-9.0	-1.0	18.0	-54
36	3.0	10.8	-8.7	-2.7	16.4	-57
37		11.0	-9.9		16.9	90
40	-52.5	-15.8		-15.8	-52.5	0
41	-20.8	-4.5	-4.0	-3.6	-21.8	13
42	-3.0	3.7	-7.0	-7.5	8.2	-58
43	5.4	8.9	-8.4	-1.5	15.9	-51
44	8.0	11.8	-8.7	1.0	18.8	-51
45	7.1	13.2	-8.2	1.4	18.9	-55
46	4.2	13.9	-7.6	0.0	18.1	-61
47		14.9	-7.5		18.1	90
50	-56.8	-17.0		-17.0	-56.8	0
51	-25.8	-6.9	-2.7	-6.5	-26.3	8
52	-7.0	0.5	-5.3	3.2	-9.7	27
53	3.1	5.3	-7.0	-2.8	11.2	-50
54	7.0	8.1	-7.3	0.2	15.0	-47
55	7.0	9.8	-7.0	1.3	15.5	-51
56	4.2	10.8	-6.1	0.8	14.4	-59
57		12.1	-5.2		14.0	90
60	-59.2	-17.8		-17.8	-59.2	0
61	-29.4	-7.4	-1.9	-7.2	-29.5	5
62	-10.5	-1.7	-4.6	0.3	-12.4	23
63	0.6	1.5	-6.1	-5.1	7.3	-47
64	5.7	3.3	-6.5	-2.1	11.1	-40
65	6.3	4.4	-5.8	-0.5	11.2	-40
66	4.0	5.2	-4.5	0.0	9.2	-49
67		6.4	-3.1		7.7	90
70	-58.4	-17.5		-17.5	-58.4	0
71	-32.0		-0.9		-32.0	0
72	-13.0		-6.4		-15.6	0
73	-0.8		-7.2		-7.7	0
74	5.3		-6.7		9.7	0
75	6.8		-5.3		9.8	0
76	4.9		-3.4		6.7	0
77						

*See figure 38 for typical grid notation.

Table VI. Moments in inch-pounds per inch for plate no. 3.
b/a = 1
a = 3 ft
p_f = 144 psf

Grid* No.	M_x	M_y	M_{xy}	M_v	M_u	θ_x (Deg.)
01	-7.1	-23.7		-7.1	-23.7	90
02	-16.1	-53.6		-16.1	-53.6	90
03	-23.8	-79.4		-23.8	-79.4	90
04	-30.6	-102.1		-30.6	-102.1	90
05	-37.2	-123.9		-37.2	-123.9	90
10	-23.7	-7.1		-7.1	-23.7	0
11	-3.5	-2.2	-10.7	7.9	-13.6	43
12	-0.3	-7.0	-12.3	9.2	-16.4	53
13	-3.3	-15.5	-11.4	3.6	-22.3	59
14	-6.7	-23.8	-10.7	-1.5	-29.0	64
15		-27.3	-11.3		-31.4	90
20	-50.0	-15.0		-15.0	-50.0	0
21	-9.6	1.7	-10.4	7.9	-15.9	31
22	4.7	9.9	-13.8	-6.8	21.4	-50
23	6.7	12.1	-13.9	-4.7	23.6	-50
24	3.8	11.6	-13.4	-6.4	21.8	-53
25		11.2	-16.5		23.1	90
30	-66.4	-19.9		-19.9	-66.4	0
31	-18.4	-1.0	-6.8	1.3	-20.7	19
32	2.8	13.8	-10.6	-3.7	20.4	-59
33	9.0	18.1	-11.8	0.9	26.2	-56
34	7.0	21.4	-11.7	0.4	28.0	-61
35		23.6	-11.9		28.6	90
40	-72.9	-21.9		-21.9	-72.9	0
41	-26.0	-5.3	-3.4	-4.7	-26.6	9
42	-2.1	6.3	-6.9	-6.0	10.2	-61
43	6.9	13.2	-8.5	1.0	19.2	-55
44	6.4	17.2	-8.4	1.9	21.8	-61
45		19.8	-7.2		22.2	90
50	-73.7	-22.1			-73.7	0
51	-31.3	-7.4	-1.5	-22.1	-31.4	4
52	-7.3	0.7	-4.8	-7.3	-9.5	25
53	3.6	5.2	-6.2	3.0	10.7	-49
54	4.9	7.7	-5.7	-2.0	12.2	-52
55		9.6	-3.8	0.4	11.0	90
60	-70.3	-21.1		-21.1	-70.3	0
61	-34.8		-0.4		-34.8	0
62	-10.7		-6.5		-13.8	0
63	2.1		-6.5		7.7	0
64	5.0		-4.5		7.6	0

*See figure 38 for typical grid notation.

26

Table VII. Moments in inch-pounds per inch for plate no. 4.
b/a = 5/4
a = 3 ft
p_f = 144 psf

Grid* No.	M_x	M_y	M_{xy}	M_v	M_u	θ_x (Deg.)
01	-8.1	-27.0		-8.1	-27.0	90
02	-19.2	-64.3		-19.2	-64.3	90
03	-29.8	-99.5		-29.8	-99.5	90
04	-39.7	-132.4		-39.7	-132.4	90
05	-49.2	-164.0		-49.2	-164.0	90
10	-27.0	-8.1		-8.1	-27.0	0
11	-6.2	-5.0	-13.5	8.0	-19.2	44
12	-2.8	-15.4	-16.5	8.6	-26.8	56
13	-6.4	-24.7	-16.0	3.0	-34.1	60
14	-10.3	-36.4	-15.6	-3.0	-43.7	65
15		-45.0	-16.1		-50.2	90
20	-60.8	-18.2		-18.2	-60.8	0
21	-15.1	-0.2	-14.3	8.5	-23.8	31
22	2.4	11.2	-13.1		26.7	-51
23	5.7	11.1	-19.9	-11.7	28.5	-49
24	3.2	10.3	-19.8	-13.4	26.9	-50
25		9.6	-24.3		29.7	90
30	-85.0	-25.5		-25.5	-85.0	0
31	-26.8	-2.5	-10.2	1.2	-30.5	20
32	0.2	13.3	-15.6	-10.2	23.7	-56
33	9.2	22.6	-17.4	-2.6	34.6	-55
34	8.1	27.5	-17.7	-2.4	37.9	-59
35		30.7	-19.0		39.8	90
40	-97.1	-29.1		-29.1	-97.0	0
41	-37.0	-6.9	-5.5	-5.9	-38.0	10
42	-5.5	9.7	-10.1	-10.6	14.8	-61
43	7.4	20.7	-12.5	-0.2	28.2	-59
44	8.1	27.4	-13.0	1.6	34.0	-63
45		31.8	-12.5		36.2	90
50	-99.9	-30.0		-30.0	-99.9	0
51	-44.1	-10.8	-1.9	-10.7	-44.2	3
52	-12.0	3.4	-5.5	5.2	-13.7	18
53	3.1	12.9	-7.9	-1.3	17.4	-61
54	6.0	18.9	-8.4	1.8	25.1	-63
55		22.6	-6.9		24.6	90
60	-97.4	-29.2		-29.2	-97.4	0
61	-48.1	-11.3	0.2	-11.3	-48.1	0
62	-17.5	-1.3	-3.3	-0.6	-18.2	11
63	-1.2	4.6	-5.4	-4.4	7.8	-59
64	3.6	8.1	-5.3	0.1	11.6	-57
65		10.5	-3.4		11.5	90
70	-88.0	-26.4		-26.4	-88.0	0
71	-50.8		2.2		-50.9	0
72	-21.2		-5.7		-22.6	0
73	-3.3		-6.2		-8.1	0
74	3.2		-4.4		6.2	0

*See figure 38 for typical grid notation

Table VIII. Moments in inch-pounds per inch for plate no. 5.
b/a = 3/2
a = 3 ft
p_f = 144 psf

Grid* No.	M_x	M_y	M_{xy}	M_v	M_u	θ_x (Deg.)
01	-8.9	-29.6		-8.9	-29.6	90
02	-22.0	-73.4		-22.0	-73.4	90
03	-35.0	-116.7		-35.0	-116.7	90
04	-47.6	-158.7		-47.6	-158.7	90
05	-59.7	-199.1		-59.7	-199.1	90
10	-29.6	-8.9		-8.9	-29.6	0
11	-8.7	-7.5	-16.0	8.0	-24.1	44
12	-5.2	-17.9	-20.2	9.7	-32.7	54
13	-9.4	-33.3	-20.3	2.4	-44.9	60
14	-13.7	-48.3	-20.0	-4.5	-57.4	67
15		-59.3	-20.3		-65.6	90
20	-69.8	-21.0		-21.0	-69.8	0
21	-20.2	-2.1	-17.8	8.9	-31.1	32
22	-0.2	6.9	-24.4	-21.3	28.1	-49
23	4.4	9.0	-25.6	-19.0	32.5	-48
24	2.4	7.8	-25.7	-20.7	30.9	-48
25		6.6	-31.4		34.9	90
30	-101.4	-30.4		-30.4	-101.4	0
31	-34.9	-4.3	-13.6	0.9	-40.2	21
32	-2.8	13.9	-20.5	-16.6	27.8	-56
33	8.9	25.1	-22.9	-6.5	40.6	-55
34	8.7	31.2	-23.5	-6.1	45.9	-58
35		35.1	-25.6		48.6	90
40	-119.6	-35.9		-35.9	-119.6	0
41	-47.7	-8.9	-8.0	-7.3	-49.3	11
42	-9.2	11.8	-13.8	-16.0	18.7	-64
43	7.5	26.1	-16.9	-2.4	36.2	-59
44	9.6	35.1	-17.8	0.5	44.3	-63
45		40.8	-17.8		47.5	90
50	-125.8	-37.7		-37.7	-125.8	0
51	-56.8	-13.4	-3.1	-13.2	-57.0	4
52	-16.5	5.9	-7.4	8.1	-18.8	17
53	3.0	19.4	-10.5	-2.1	24.5	-64
54	7.5	28.6	-11.5	2.3	33.8	-66
55		34.1	-10.5		37.0	90
60	-124.1	-37.2		-37.2	-124.1	0
61	-61.9	-16.2	0.3	-16.2	-61.9	0
62	-23.2	-0.3	-2.7	0.1	-23.5	7
63	-2.5	10.8	-5.5	-4.5	12.8	-70
64	4.2	17.9	-6.6	1.5	20.6	-68
65		22.0	-5.1		23.2	90
70	-117.1	-35.1		-35.1	-117.1	0
71	-63.7	-14.7	2.5	-14.6	-63.9	-3
72	-28.4	-3.4	-0.8	-3.3	-28.5	2
73	-7.4	3.3	-3.3	4.2	-8.2	16
74	1.2	7.3	-3.8	-0.6	9.2	-65
75		9.6	-2.2		10.1	90
80	-100.6	-30.2		-30.2	-100.6	0
81	-65.2		5.4		-65.6	0
82	-32.2		-3.7		-32.6	0
83	-9.8		-4.8		-11.8	0
84	0.3		-3.6		3.7	0

*See figure 38 for typical grid notation.

Publications of the
Iowa Engineering Experiment Station

The Iowa Engineering Experiment Station publishes reports of the results of completed projects in the form of technical bulletins. Other research results are published in the form of Engineering Reports.

Single copies of publications not out of print may be obtained free of charge, except as noted, upon request to the Director, Iowa Engineering Experiment Station, Ames, Iowa. The publications are available in many libraries. *Indicates out of print.

BULLETINS

No. 176.   Constants for Design of Continuous Girders with Abrupt Changes in Moments of Inertia. R. A. Caughey and R. S. Cebula. 1954.

No. 177.   Elastic Stability of the Top Chord of a Three-Span Continuous Pony Truss Bridge. Frank Kerekes and C. L. Hulsbos. 1954.

No. 178.   Universal Swing Curves for Two Machine Stability Problem with Multiple Switching. A. A. Fouad and W. B. Boast. 1956. ($1.00)

No. 179.   The Survival of Swine Disease Organisms in the Heat Treatment of Garbage. E. R. Baumann, R. A. Packer, et al. 1957. ($1.45)

No. 180.   Colorimetric Characteristics of Color Television Images Recorded on Black and White Film. W. L. Hughes. 1957. ($0.50)

No. 181.   Parking Practices on College Campuses in the United States. L. H. Csanyi. 1958. ($0.50)

No. 182.   Structural Behavior of a Plate Resembling a Constant Thickness Bridge Abutment Wingwall. H. P. Harrenstien and W. C. Alsmeyer. 1959. ($0.75)

No. 183.   Moment Contours for Bridge Abutment Wingwalls of Constant Thickness. C. L. Hulsbos and W. H. McCasland. 1959. ($0.75)

ENGINEERING REPORTS

No. 23.   Secondary Stresses in Buried High Pressure Lines. M. G. Spangler. Reprint. 1954-1955.

No. 24.   The Use of Good English in Technical Writing. J. H. Bolton. Reprint. 1954-1955.

No. 25.   Fertilizer Research, Part I. G. L. Bridger and associates. Reprints. 1955-1956.

No. 26.   Bond Between Concrete and Steel. H. J. Gilkey, S. J. Chamberlin, and R. W. Beal. Reprints. 1956-1957. ($1.85)

No. 27.   Fertilizer Research, Part II. G. L. Bridger, D. R. Boylan and associates. Reprints. 1957-1958. ($0.75)

No. 28.   Plastics as Materials of Construction. L. K. Arnold. Reprint. 1957-1958. ($0.25)

No. 29.   Flexural Strength of Hollow Unit Concrete Masonary Walls in the Horizontal Span. A. R. Livingston, et al. 1958-1959. ($0.50)

No. 30.   Alcoholic Extraction of Vegetable Oils. R. K. Rao, L K. Arnold and associates. Reprints. 1958-1959. ($0.75)

THE COLLEGE

The Iowa State College of Agriculture and Mechanic Arts conducts work in five major fields:

Agriculture

Engineering

Home Economics

Science

Veterinary Medicine

The Graduate College conducts research and instruction in all these fields.

Four-year and five-year collegiate curricula are offered in the different divisions of the College. Non-degree programs are offered in agriculture. Summer sessions include graduate and collegiate work. Short courses are offered throughout the year.

Extension courses are conducted at various points throughout the state.

The College has five special research institutions: the Agricultural and Engineering Experiment Stations, the Veterinary Medical and Industrial Science Research Institutes, and the Institute for Atomic Research.

Special announcements of the different branches of the work are supplied, free of charge, on application.

Address, THE REGISTRAR, THE IOWA STATE COLLEGE, Ames, Iowa.